# Measurement report: Characterization of uncertainties of fluxes and fuel sulfur content from ship emissions at the Baltic Sea

Jari Walden[1], Liisa Pirjola[2,3], Tuomas Laurila[1], Juha Hatakka[1], Heidi Pettersson[4], Tuomas Walden[1], Jukka-Pekka Jalkanen[1], Harri Nordlund[2], Toivo Truuts[5], Miika Meretoja[6], Kimmo K. Kahma[4]

[1]Climate Research Program, Finnish Meteorological Institute, Helsinki, Finland
[2]Department of Automotive and Mechanical Engineering, Metropolia University of Applied Sciences, Vantaa, Finland
[3]Aerosol Physics Laboratory, Faculty of Engineering and Natural Sciences, Tampere University, Tampere, Finland
[4]Meteorological and Marine Research Program, Finnish Meteorological Institute, Helsinki, Finland
[5]Air Quality Management Department, Estonian Environmental Research Centre, Tallinn, Estonia
[6]City of Turku, Turku, Finland

*Correspondence to*: Jari Walden (jari.a.walden@gmail.com)

**Abstract.** Fluxes of gaseous compounds and nanoparticles were studied by micrometeorological methods at Harmaja in the Baltic Sea. The measurement site situated by the ship route to and from the city of Helsinki. The gradient method (GR), was used to measure fluxes of $SO_2$, NO, $NO_2$, $O_3$, $CO_2$, and $N_{tot}$ (number concentration of nanoparticles). In addition, the flux of $CO_2$ was also measured by the eddy covariance method (EC). Distortion of the flow field caused by obstacles around the measurement mast was studied by applying a computation fluid dynamic (CFD) model. This was used to establish the corresponding heights in the undisturbed stream, and the wind speed as well as the turbulent parameters at each of the established heights were recalculated for the gradient model. The effect of waves on the boundary layer was taken into consideration, because the Monin–Obukhov theory used to calculate the fluxes is not valid in the presence of swell. Uncertainty budgets for the measurement systems were constructed to judge the reliability of the results. No clear fluxes across the air-sea nor sea-air interface were observed for $SO_2$, NO, $NO_2$, $NO_x$ (= NO + $NO_2$), $O_3$, and $CO_2$ by the GR method. A negative flux was observed for $N_{tot}$ with a median value of $-0.23 \times 10^9$ m$^{-2}$ s$^{-1}$ with an uncertainty range of 31-41 %. For $CO_2$, while both positive and negative fluxes were observed, the median value was -0.0036 mg m$^{-2}$ s$^{-1}$ with uncertainty ranges of 30-60 % for the EC methods. Ship emissions were responsible for deposition of $N_{tot}$ while they had a minor effect on $CO_2$ deposition. The fuel sulfur content (FSC) of the marine fuel used in ships passing the site was determined from the observed ratio of $SO_2$ and $CO_2$ concentrations. A typical value of $0.40 \pm 0.06$ %, was obtained for FSC, which is in compliance with the contemporary FSC limit value of 1 % in the Baltic Sea Area at the time of measurements. The method to estimate the uncertainty of FSC was found to be accurate enough for use with the latest regulations, 0.1 % (Baltic Sea Area) and 0.5 % (Global Oceans).

**1 Introduction**

30    The Baltic Sea, due to its nature as a relatively small inland sea with heavy ship traffic and a large population around the sea, is very sensitive to pollutants. Due to the very narrow and shallow strait of Kattegat in Denmark, the exchange of seawater between the North Sea and the Baltic Sea is limited. The load of phosphorus and nitrogen in the Baltic Sea mainly comes through the rivers. The rivers bring in fresh water, maintaining the salinity of the seawater in the Baltic Sea at 1/10 of that of the ocean. In addition, the airborne deposition of pollutants from the emissions of ships, and from industry, are becoming more

35    and more important sources (Hongisto and Joffre, 2005). Ship emissions of most of the air pollutants except CO have decreased during 2006-2018, but greenhouse gas emissions from ships have remained stable throughout the period, regardless of the growth of ship transport reported in tonne kilometres (HELCOM, 2019). Ship emissions enter the sea mostly by indirect deposition of sulfur and nitrogen compounds through chemical conversion in the atmosphere (de Leeuw et al., 2003; Hongisto et al., 2005; Hongisto, 2014), or by direct deposition from the gas phase. In the Batic Sea few measurement facilities to measure

40    the gas exchange between the sea-air interface by micrometeorological methods has been set up (Smedman et al. 1999, Honkanen et al. 2018). The need for reduction of atmospheric pollutants in the emissions has been taken seriously within the International Maritime Organization (IMO), which launched the MARPOL agreement for reduction of ship emissions, Annex VI (IMO, 1997). The latest revision includes more stringent emission limits for $NO_x$ and $SO_2$. In spite of these abatement regulations, the ship emissions of IMO registered vehicles and non-IMO registered vehicles show constant or slightly

45    increasing trends for the compounds $NO_x$, $SO_2$, and $PM_{2.5}$, as well as a clearly increasing trend for CO. Once the stringent regulation for fuel sulfur content (FSC) in marine fuel came into power in 2014, the emissions of $SO_2$ and $PM_{2.5}$ decreased rapidly at regional and global level (Johansson and Jalkanen, 2016; Johnsson et al 2020; Seppälä et al. 2020).

The goal of this study was (i) to measure the gas and nanoparticle exchange between the sea-air interface in marine coastal environment close to the ship routes, (ii) to study the transport and dispersion of the ship plume to the footprint area, (iii) to

50    define the FSC from the ship emission plumes and (iv) to characterise the uncertainty sources of the measurement results. The measurements took place at the Baltic Sea at the small island of Harmaja in the vicinity of the city of Helsinki during the summers of 2011 and 2012. The ship routes between the city of Helsinki and the cities of Tallinn, Stockholm and St. Petersburg pass by the measurement site. The exchange of the gaseous $NO_x$, $SO_2$, $CO_2$, $O_3$, and fine particles across the sea and atmosphere surface layer was studied by micrometeorological methods. The fluxes of these compounds were measured by the gradient

55    method and the eddy covariance method. In addition, concentration of methane was measured. The major sources of the pollutants were ship emissions, but also trans-boundary emissions as well as emissions from the sea and from the city of Helsinki contributed to the observed concentration levels of the pollutants. The FSC of the ships' marine fuel was determined from the measured concentrations of $SO_2$ and $CO_2$ (Cooper et al., 2005) to determine the compliance of the fuel used with the regulation. The ships passing the measurement site were identified by using AIS data (Jalkanen et al., 2009). This method has

60    been demonstrated for defining the FSC in studies (Alföldy et al., 2013; Moldanova et al., 2013; Pirjola et al., 2014). Since recently, it has already been used as an indicator method for purposes of routine control by the authorities in some countries

(Mellquist, 2018). The uncertainty of the flux and FSC measurements were estimated based on the performance of the analyzers and measurement probes for meteorological parameters, for FSC the uncertainty of defining the peak areas of emission plumes from the ships was also taken into account.

65

## 2 Theoretical background

### 2.1 Micrometeorological methods

The micrometeorological methods are used for measuring gas exchange across the surface layer (Kaimal and Finnigan, 1994); of these the eddy covariance method (EC) and the gradient method (GR) are commonly used. The use of micrometeorologocal
70   methods reguires criterias to fulfil for the atmospheric conditions being similar for both methods. As such stationarity of the flux measurements, the footprint area and the occurrence of swell were considered. The eddy covariance method is a direct flux measurement method, while the gradient method is an indirect measurement method. In the eddy covariance method the flux of a gas compound is measured by using fast sensors (response better than 10 Hz) to measure the fluctuation of wind velocities and the concentration of chemical compounds. The gradient method overcomes the problems of fast analysis of
75   chemical compounds. On the other hand, this method requires that the atmospheric conditions are stationary, and it also needs very accurate measurements of the parameters it uses (Businger, 1986), as well as the assumption of constant layer flux (Dyer and Hicks, 1970). In this study both the GR and the EC methods were used. The gradient method was used for the gas compounds (oxides of nitrogen, ozone, sulfur dioxide and carbon dioxide) as well as for nanoparticles. The eddy covariance method was used to measure the flux of carbon dioxide. In the GR method the wind speed should be measured at different
80   heights, usually with conventional cup anemometers, while in the EC method the fluctuation of the 3-dimensional wind speed is measured by a sonic anemometer. Short descriptions of both methods are given below, with more emphasis laid on the gradient method.

$$F_c = -K_c \frac{\partial c}{\partial z} \tag{1}$$

where $F_c$ is the flux of the scalar quantity $c$, $K_c$ is the eddy diffusivity of $c$; $c$ means here the gas compounds and particles. The
85   gradient $\partial c/\partial z$ describes the mean concentration of c in the vertical direction $z$. By definition, the flux is opposite to the gradient, which is positive towards the increasing concentration. The eddy diffusivity for a chemical compound $c$ is calculated by applying an assumption $K_C = K_h$, (Businger 1986) i.e. the eddy diffusivity of gas concentration is the same as that for heat. The eddy diffusivity for heat transfer can be expressed as:

$$K_h = k \cdot u_* \cdot z / \phi_h \tag{2}$$

90   where $\phi_h$ is the dimensionless temperature gradient. Eq. (1) can now be rewritten with the help of Eq. (2) in the form

$$F_c = -\frac{k u_* z}{\phi_h} \frac{\partial c}{\partial z} \tag{3}$$

where $k$ is the von Karman constant ($\approx 0.4$), $u_*$ is the friction velocity, $c$ is the concentration of the chemical compound, and the dimensionless temperature gradient $\phi_h$ is defined as

$$\phi_h = \frac{kz}{\theta^*}\frac{\partial\overline{\theta}}{\partial z} \tag{4}$$

Here $\theta$ is the potential temperature (Panofsky and Dutton, 1987) and $\theta^*$ ($= -\overline{\theta'w'}/u_*$) is the scaling parameter for temperature. The dimensionless potential function, Eq. (4), can be written in a way similar to the momentum $\phi_m$ and for the concentration of a chemical species (gases and particulate matter) $\phi_i$, respectively. The line above the symbol means the average of the quantity over time. Eq. (3) can be presented in the form

$$Fc = -\frac{ku_*(c(z_2)-c(z_1))}{\left(\ln\left(\frac{z_2}{z_1}\right)-\Psi_c(\zeta_2)+\Psi_c(\zeta_1)\right)} \tag{5}$$

where $\psi_c(\xi_2)$ and $\psi_c(\xi_1)$ are the integral functions of Eq. (4) over the stability parameter $\xi$ at heights $z_2$ and $z_1$. The dimensionless gradient function Eq. (4) can be represented in the semi-empirical form of Businger and Dyer (Businger et al., 1971; Dyer, 1974), which is used here for the calculations. The stability parameter $\xi$ is related to the Monin-Obukhov (M-O) length, $L$, according to the relation $\xi = z/L$, where $z$ is the height from the surface. Eq. (5) is valid in neutral ($\xi = 0$) and unstable ($\xi < 1$) conditions, but not in stable conditions ($\xi \gg 1$) (Panofsky and Dutton, 1987).

In Eq. (5) the concentration difference at heights $z_2$ and $z_1$ is known from the measurements, but the friction velocity, the integral functions ($\psi_c$), and the stability parameter are unknown. To solve the turbulence parameters, a method proposed by Paulson (Paulson, 1970) was applied.

On the other hand, the sonic anemometer measures the wind velocity with the help of acoustic pulses that propagate along the path between the sound emitter and the receiver. The three-dimensional wind components, i.e. horizontal ($u$, $v$) and vertical ($w$), are measured based on the changes in the acoustic signals along the fixed path lengths. The momentum flux $F_m$ measured by the sonic anemometer can be calculated from the expression

$$F_m = \rho\overline{u'w'} = \rho u_*^2 \tag{6}$$

where $\rho$ is the air density, $u'$ and $w'$ are the fluctuations of the wind speed components measured by the sonic anemometer, and $u_*$ is the friction velocity. The friction velocity can be calculated from the surface stress according to

$$u_* = \left(\overline{-u'w'}\right)^{1/2} \tag{7}$$

Once the friction velocity is calculated according to Eq. (7), the Monin-Obukhov length can be expressed:

$$L = -\frac{u_*^3\theta}{kgQ_{*o}} = -\frac{u_*^3 T}{kg\overline{w'T'}} \tag{8}$$

where $\theta$ is the potential temperature (in K), g is the acceleration of gravity and $Q_{*o}$ is the heat flux at the surface. The right side of eq. (8) is an approximation where $T$ is the air temperature, $\overline{w'T'}$ is the heat flux measured by sonic anemometer. The

120 friction velocity and the M-O length obtained from the sonic measurements were used to complete the solutions for the the GR method. The M-O similarity theory states that the mean and turbulence variables in the surface layer are functions of height near the ground. General conditions for the M-O similarity theory are horizontally homogeneous surface structure, stationary (or near stationary) condition (e.g. Foken and Wichura, 1996), constant flux layer and that the atmospheric turbulence is affecting on the vertical profiles of wind speed, potential temperature and humidity. In addition to the conditions above, at

125 marine environment the M-O similarity theory has been found to be valid over slowly moving waves, which sufficiently resemble solid ground, but it fails in the presence of swell, i.e. waves that move faster than the wind (e.g. Drennan at al., 1999; Smedman et al., 1999). The effects of swell on the boundary layer are manifold (Högström et al., 2008, 2013, 2015), the most conspicuous being the absence of a vertical velocity gradient above a certain wavelength-dependent height. From the results of Kahma et al. (2016) it can be deduced that the absence of wave components that are faster than the wind speed at 10 m

130 height is typically sufficient to ensure that the waves do not invalidate the M-O similarity theory.

   Similarly to the momentum flux in Eq. (6) one can express the vertical flux of a gas compound, e.g. $CO_2$, by

$$F_c = \overline{\rho_a} \overline{w'c'} \tag{9}$$

where $\rho_a$ is the density of dry air, and $c'$ is the measured molar fraction of $CO_2$ ($\mu$mol mol$^{-1}$). The commonly used infra-red analyzers measure the concentration of $CO_2$ in air normally in wet condition unless an air drier is used in the sampling tube.

135 The widely used method to correct the fluctuations of water vapour and heat is the so called WPL method proposed by Webb et al. (1980), which is applied in this study.

## 2.2 NO-O₃-NO₂ chemistry

The chemical interconversion of the system NO - O₃ - NO₂ is well-known and described in the literature (Seinfeld and Pandis, 2012). In the atmosphere the reaction system NO - O₃ - NO₂ forms a cycle where the reaction forming NO₂, i.e., the reaction

140 NO + O₃ is the reverse of the reaction for dissociating NO₂ to form NO, which takes place in the presence of sunlight (at wavelengths < 420 nm).

   The chemical cycle in the NO − O₃ − NO₂ system is fast depending on the concentration of the compounds but also on the available sunlight (day/night time). The time scale ($t$) for vertical mixing can be estimated from the relation, $t = z/u_*$. With z as 10 m and the friction velocity between 0.1 to 0.5 m/s, the time scale for vertical mixing is 20 to 100 s. This is of the same

145 order of magnitude as the time scale of the NO − O₃ − NO₂ system. Therefore, the assumption of vertical constant flux according to M-O theory is not valid. The approximation $K_h = K_c$ is not correct, and therefore the turbulent exchange coefficient $K_c$ (Eq. (2)) must be modified. This problem has been discussed by several authors (Lenschow and Delany, 1987; Kramm et al., 1991; Vila-Guerau de Arellano et al., 1993; Duyzer et al., 1995). Lenschow and Delany (1987) constructed an analytical formulation for the flux profiles of the NO and NO₂ compounds as a function of height. Duyzer et al (1995) developed a correction

150 procedure for the formula of Lenschow and Delany.

**2.3 Estimation of the sulfur content in the marine fuel of the ships**

The maximum sulfur content in the marine fuel used on the oceans is defined in the Annex VI of the MARPOL agreement (IMO, 2007). The agreement also defines the sea areas where a lower content of sulfur in the marine fuels must be used. These restricted sea areas, called SOx Emission Control Areas (SECA) need to be approved by the countries in the proposed SECA.

155   The Baltic Sea and the North Sea (IMO, 2007) form a SECA area, where the stringent sulfur limit for the marine fuels applies. In 2012, the EU updated the directive (Directive 1999/32/EU) to include the more stringent demands from MARPOL Annex VI (Directive 2012/33/EU). According to the MARPOL Annex VI the testing of sulfur content shall be in accordance with the ISO standard, which includes a set of key tests, e.g. to identify potential fuel issues where exceedances of emission may occur (ISO 8217:2012). According to ISO 8217 the standard method for the assessment of the sulfur content shall be in accordance

160   with the ISO 8754 (ISO 8754:2003). The main issue here is that the sample for the analysis of the sulfur content needs to be taken from the bunker fuel at the harbour, not during the cruise.

A method that can be used to determine the FSC during the cruise is to measure the ratio of $\Delta SO_2$ to $\Delta CO_2$ from the emissions, either from the stack or from the ambient air. The $\Delta SO_2$ and $\Delta CO_2$ are the integrated peak concentrations of $SO_2$ and $CO_2$ when the background concentrations are subtracted i.e. $\Delta C = C_{peak} - C_{bg}$. By assuming that all sulfur in the fuel has

165   been oxidized to $SO_2$, the FSC can be calculated according to e.g. (10) (Pirjola et al. 2014):

$$FSC\ (\%) = \frac{\frac{\Delta SO_2\ (ppb)}{10^3} \cdot M_S}{\Delta CO_2\ (ppm) \cdot M_{CO2}} \cdot EF_{CO2} \cdot 100 = \frac{\Delta SO_2\ (ppb)}{\Delta CO_2\ (ppm)} \cdot 0.23 \tag{10}$$

where $M_S$ and $M_{CO2}$ are the mole masses of S and $CO_2$, and $EF_{CO2}$ is the emission factor for $CO_2$. Here the value of 3.107 kg $CO_2$ per kg fuel burned was used (Petzold et al., 2008).

Eq. (10) yields lower limits for FSC (Williams et al., 2009) since a small part of the sulfur in the fuel, less than 6 % (Alföldy

170   et al., 2013) or 0.7 % (Moldanova et al., 2013), might be emitted as $SO_3$ or converted to $H_2SO_4$ by homogeneous and heterogeneous pathways in the atmosphere.

**2.4 Uncertainty estimates**

The uncertainty in the measurements is one of the most important issues to solve when analysing the results. The measurements are influenced by a number of error sources that need to be identified and quantified, e.g. the performance characteristics of

175   gas and particle analyzers and the different probes and sensors used for the measurements. Besides the uncertainties associated with the instruments, the EC and GR methods are very sensitive with respect to the topography and the atmospheric conditions. In particular, the stochastic nature of turbulence (Lenschow et al., 1994; Rannik et al., 2006) and the noise present in the measured signals cause random errors (Lenschow and Kristensen, 1985, Rannik et al., 2016), which are difficult to estimate. However, a number of error sources have been identified that have an influence on the results of flux measurement by the EC

180   method (Businger 1986, Rinne et al 2000). The statistical error of an EC estimate is usually quite large.

The uncertainty sources that contribute to the uncertainty of the flux results by the GR method are systematic and random in nature. Calibration of the response of all instruments, correction of the humidity for $CO_2$ analyzers and cross-calibration due to sampling tubes of the analyzers are systematic errors. All the uncertainty sources (systematic and random) that contribute to the results need to be corrected. Even after correction for all systematic errors, there is always a residual component that needs to be included in the uncertainty budget. The residuals are estimated according to the best knowledge available. The variance of the standard uncertainty can be expressed in the form (JCGM, 2008)

$$u_c{}^2 = \sum_{i=1}^{n} (\frac{\delta f}{\delta w_i})^2 u_i{}^2 + 2 \sum_{i=1}^{n-1} \sum_{j=i+1}^{n} \frac{\delta f}{\delta w_i} \frac{\delta f}{\delta w_j} u_i u_j \rho_{ij} , \tag{11}$$

where the square root of $u_c{}^2$ is the combined standard uncertainty. It includes all the uncertainty components $u_i$ (standard uncertainties) of the function $f$ describing the measurement quantity in question for each of the parameters $w_i$ associated with the results of the measurements. The covariance term (the second term on the right-hand side) in Eq. (11) needs to be taken into account when it is about the same order of magnitude as the independent part in Eq. (11). Once the combined standard uncertainty has been determined, the expanded uncertainty U can be calculated according to $U = k \cdot u_c$. Here a factor of $k = 2$ was used representing the 95 % confidence level of a normal distribution. In the case of the gradient method the uncertainty sources contributing to the fluxes associated with the method can be expressed by applying Eq. (2) to Eq. (11). For simplicity the covariance terms in Eq. (11) have been ignored since they are of the second order of magnitude.

The combined standard uncertainty of the flux of a compound $c$ can then be approximated in the form:

$$\frac{u_c(F_c)^2}{F_c^2} = \frac{u(u_*)^2}{u_*^2} + \frac{u(\Psi_h)^2}{(\ln(\frac{z_2}{z_1}) - \Delta\Psi_h)^2} + \frac{u(\Delta c)^2}{\Delta c^2} + \frac{u(z)^2}{(\ln(\frac{z_2}{z_1}) - \Delta\Psi_h)^2} (\frac{1}{z_1^2} + \frac{1}{z_2^2}) + u(ws)^2. \tag{12}$$

The standard uncertainties are calculated according to Eq. (11) for each of the contributors in Eq. (12): the friction velocity, the integral functions of the Businger-Dyer functions, the concentrations of gases and particles, as well as the measurement heights and the wind speed (ws). The estimated relative uncertainties for each of the contributing sources of uncertainty are presented in Supplementary Table S1.

The combined standard uncertainty of the fuel sulfur content $u_c$ (FSC) is estimated by applying Eq. (10) to Eq. (11), and it can be expressed in the form:

$$(\frac{u_c(FSC)}{FSC})^2 = (\frac{u(SO_2)}{\Delta SO_2})^2 + (\frac{u(SO_{2,bg})}{\Delta SO_{2,bg}})^2 + (\frac{u(CO_2)}{\Delta CO_2{}^2})^2 + (\frac{u(CO_{2,bg})}{\Delta CO_{2,bg}{}^2})^2 , \tag{13}$$

where $u(SO_2)$ and $u(CO_2)$ are the standard uncertainties of the measured $SO_2$ and $CO_2$ concentrations at the peak area concentration, while $u(SO_{2,bg})$ and $u(CO_{2,bg})$ are the standard uncertainties of the background concentrations.

# 3 Measurements and data analysis

## 3.1 The measurement site and the meteorological parameters

The first measurement campaign at Harmaja (60°06´18.166´´N, 24°58´28.808´´E) started on July 13 after installation of the measurement instruments, and it ended on October 12, 2011. The second campaign started on July 7 and ended on August 20, 2012. The isle of Harmaja is a pilot station located in the Gulf of Finland, about four kilometres from the city of Helsinki in Finland. The ship routes both from Tallinn to Helsinki and from Stockholm to Helsinki pass by the isle of Harmaja at distances of 1 km and 100 – 200 m, respectively, as shown in Fig. 1. Fig. 1 also shows the modelled NOx emissions.

The measurement station (Fig. 2) was set up in an old military fire control tower made of steel and concrete. All the measurement instruments were installed inside the tower, while measurement probes and sampling inlets were installed at different heights in a mast beside the tower. The height of the mast was 9 m, and it was standing on a breakwater 3.5 m above mean sea level (MSL). The measurement probes were installed at different heights to get an extensive view of the meteorological quantities. Cup anemometers by Vaisala (WAA 15 cup anemometers, Vaisala, Finland) measured the wind speed while the turbulence parameters were measured by an ultrasonic anemometer by METEK (Ultrasonic Wind Sensor uSonic-3 Scientific, METEK GmbH, Germany). Pt-100 sensors measured the ambient temperature. The cup anemometers were installed at three different heights, 12.2 m, 10.9 m, and 9.9 m above MSL. The sonic anemometer was installed at the top of the mast at a height of 12.9 m, and the temperature probes were installed at heights of 12.3 m, 11.0 m, and 10.0 m. The sampling intakes for the gaseous compounds were installed at two different heights, 12.58 m and 9.98 m. The inlets for particle measurements were installed at 8.0 m and 10.0 m. Next to this mast the official weather mast of the FMI (Fig. 2) was standing, equipped with a cup anemometer (WAA 15 wind vane, Vaisala, Finland) and a wind direction vane by Vaisala (WAV-15) at a height of 16.6 m. The current sea level was measured as a 30 min average with reference to MSL. The measurement heights of the probes used in the calculations are from the current sea level.

## 3.2 Instrumentation

The atmospheric concentrations of ozone, oxides of nitrogen and sulfur dioxide were measured simultaneously by conventional gas analyzers intended for ambient air quality measurement. Two identical analyzers of each gas were used to detect the concentration at the two measurement heights (12.58 m and 9.98 m). The sampling tubes at each altitude were made equal in length. PTFE (Polytetrafluoroethene) was used as tube material, since it is an inert material for each of the gaseous pollutants. The measurement method for ozone was the UV-photometric method (EN 14625:2012), and it was performed with APOA-360 analyzers by Horiba, Japan. For nitrogen oxides ($NO_x$) the chemiluminescence method was used (EN-14211:2012) and the measurements were performed with the AC31M analyzer by Environnement S.A., France. The AC31M analyzer was constructed as a two-channel instrument that measures the concentration of NO and $NO_2$ simultaneously. For sulfur dioxide the UV-fluorescence method (EN-14212:2012) was used and measured with a TEI 43 CTL analyzer by Thermo Environment. LI-7000 by Licor was used for the EC method to measure the concentration of $CO_2$ and $H_2O$. Picarro G2301 by Picarro Inc

measured the concentration of $CO_2$, $CH_4$ and $H_2O$. Results of the LI-7000 and the Picarro G2301 were also used for calculating the $CO_2$ flux with the GR method.

For particle sampling stainless steel tubes with an outer diameter of 12 mm were used. Particle number concentration and size distribution were measured by two ELPIs (Electrical Low Pressure Impactor, Dekati Ltd.) (Keskinen et al., 1992); ELPI1 measured at 10.0 m and ELPI2 at 8.0 m height. The measurement principle of both ELPIs was the same: particles were first charged and then classified into 12 stages according to their aerodynamic diameter, in the size range of 7 nm–10 μm. Both ELPIs were equipped with a filter stage (Marjamäki et al., 2002), and ELPI1 additionally with an extra stage designed to enhance the particle size resolution for nanoparticles (Yli-Ojanperä et al., 2010). The cut-off diameters were 0.016 (additional stage, only in ELPI1), 0.030, 0.056, 0.093, 0.156, 0.264, 0.385, 0.617, 0.954, 1.610, 2.410, 4.04 (only in ELPI2) and 9.97 μm. The mass concentration of particles smaller than 1 μm ($PM_1$) was calculated by assuming the particles to be spheres with a density of 1000 $kg/m^3$.

The strategy for the air quality measurements in 2012 was different, and it included measuring concentrations of NO, $SO_2$, $CO_2$, $O_3$, and particles at one height, and $CO_2$ fluxes by the EC method. The $NO_x$ analyzer was a modified version of a single channel analyzer, Thermo 42 CTL by Thermo Environment. The modification was made by bypassing the $NO_2$ converter and the solenoid valve, increasing the flow rate by choosing an orifice which allowed a flow rate of up to 2 l/min, and by using the shortest integration time. The purpose of the modification was to make the analyzer faster for detecting the emission peaks of the ships, but for the NO gas only. The $SO_2$ analyzer was also a modified version from TEI 43 CTL by Thermo Environment. The purpose of modification was the same as in case of $NO_x$ analyzer: to make it faster for detecting ship emissions. The $O_3$ and $CO_2$ analyzers and the particle analyzer (ELPI1) were the same as in the 2011 campaign.

**3.3 Calibration of the instruments**

The temperature probes (Pt-100) were calibrated at the FMI in the calibration laboratory for meteorological quantities. The wind speed anemometers were serviced (cleaned and the ball bearings changed) in the same laboratory. The gas analyzers were calibrated in the reference calibration laboratory at the FMI before and after the field campaign. The calibration laboratory is responsible for the tasks of the national reference laboratory on air quality, and it conducts the calibrations of the air quality analyzers and calibration facilities in Finland. The laboratory maintains the traceability of the calibration to the SI units, and it is accredited according to ISO 17025:2005 for all measured gas compounds except $CO_2$. The dynamic dilution method by accurate gas sources was used for the calibration (Haerri et al. 2017). The calibration concentrations were selected to cover the expected measurement ranges for each of the gas components.

The analyzers were also calibrated at the measurement site during the campaign using a field calibration unit similar to that in the laboratory. Both ELPIs were factory calibrated and serviced. Zero setting and HEPA filtration tests were performed before and after each measurement period. Based on the parallel measurements of the ELPIs on 30.8.2011 and 2.9. 2011 correction factors were inferred for ELPI2, separately for each stage (dN/dlogDp), and for the number concentration of particles smaller than 1μm ($N_{tot}$) that was used for the flux calculations (more details in Supplement). All measured Ntot data from the

ELPI2 were corrected accordingly. This ensures that the results are correct within the stated uncertainty and are comparable with the other similar measurements.

### 3.4 Data acquisition systems and data analysis

275 The data acquisition systems consisted of several components. The meteorological measurements were collected and stored by a Milos 500 system (by Vaisala). The ambient air quality gas analyzers were connected to a data collection system EnviDas 2000 (by Envimetria, Israel), the sonic anemometer and the LI-7000 were connected to a fast data acquisition system; Picarro G2301 used the system provided by the manufacturer, and the ELPI software was used for the collection of particle data.

The times, in EET (+2 UTC), of the different data acquisition systems were synchronized during each calibration and
280 maintenance event. The final adjustment of all data sets at each of the altitudes was made manually from the time series so that the obvious peaks coincided. Data collection for the EC method was performed at 10 Hz time resolution. In the case of the GR method, data was collected as 15 second and one minute averages, while the total number concentration of particles in the size range of 7-1000 nm ($N_{tot}$) and $PM_1$ were collected at 10 second intervals. The meteorological data from the official weather mast were collected as 10 min averages. A consistent data set was formed as 30 min averages from the synchronized
285 individual data acquisition systems.

The first target for the data analysis was to achieve accurate and good quality continuous time series for the gaseous compounds and particles at each of the measuring heights. Secondly, the turbulence parameters (M-O length, stability parameter, friction velocity) were needed for calculating the transfer coefficients $K_m$ and $K_c$, the dimensionless gradient, and their integral functions for heat and momentum, and for calculating the fluxes of the chemical compounds and fine particles.
290 The friction velocity and the M-O length, which were calculated from the data obtained by the sonic anemometer, were used as input parameters for the GR method. The benefit of this was to reach better agreement with the flux parameters.

### 3.5 Measurements on R/V Aranda

In 2012 measurements were also made on the Finnish research vessel Aranda during two days. The ship was kept stationary at a point approximately 2 km SSW from the measuring mast at Harmaja, with no islands between Harmaja and the ship. The
295 bow of the ship was equipped with a sonic (Metek USA-1), an open path LI-7500 and an enclosed path LI-7200 at two heights (10 and 16 m) for the measurement of the $CO_2$, $H_2O$, momentum and heat fluxes. During the measurements the ship's bow was kept within +/- 20 degrees into the wind direction. The sonic measurements were corrected for ship motions with a motion sensor MRU6, according to Drennan et al. (1994). In this study the measurements from the sonic and enclosed path LI-7200 at the height of 16 m were used, and the calculated fluxes were corrected for water vapour fluctuations according to Webb et
300 al. (1980). The partial pressure of $CO_2$ in the surface water at a depth of 4 m obtained from the ship's flow-through system was measured continuously with an equilibrator and a LI-6262. The measurements were transformed to *in situ* water temperature according to Takahashi et al. (1993). All the LI-CORs were calibrated against 0, 364, and 700 ppm $CO_2$ gases.

## 4 Results

### 4.1 General overview

305 Environmental factors, e.g. the fire control tower, caused challenges with regard to the measurement signals. Though the measurement probes were installed at different heights above the top of the tower the measurement signals were affected by disturbances in the flow field. Therefore a computational fluid dynamic (CFD) program OpenFOAM (version 7) by the OpenFOAM Foundation (OpenFOAM, 2020) was used to determine the amount of distortion and the required correction. OpenFOAM is a C++ based open source software developed mostly, but not exclusively, for CFD. The airflow around the

310 shoreline and the measuring structure was modelled using steady, incompressible, single-phase potential flow. The simulation covered a 80 m long, 40 m wide and 30 m high rectangular box around the measurement area.

Fig. 3a illustrates the calculated wind field isopleths at a wind speed of 9 m/s over the open sea area, and it shows how the flow field is disturbed around the measurement mast. Based on the calculated isoplets we determined for each measurement height the corresponding height over the open sea. The actual heights of wind speed probes are shown at the measurement

315 mast on the right and their projected heights over open sea on the left. The heights at the measurement masts for wind speed measurements were reduced from 16.63 m, 12.88 m, 12.18 m, 10.88 m and 9.88 m, to 15.5 m, 11,1 m, 10.2 m, 8.6 m and 7.2 m, respectively. Similarly, the heights of the sample intakes were reduced from 12.88 m, 12.58 m, 10 m, 9.88 m and 8 m down to 11,1 m, 10.7 m, 7.38 m, 7.2 m and 4.7 m, respectively. The correction for the wind speed was calculated from different simulations varying the wind speed and comparing the calculated results at the measurement mast with the open sea area.

320 These calculations show that a linear relationship for the wind distortion at the measurement mast as compared with the open sea area was good enough to correct the observed wind speed measurement at all heights. The recalculated wind speed profiles (six profiles, cases 1 to 6) at each of the corrected measurement heights are presented as averages over short periods (2 to 3 hours) in the wind sector to the open sea, i.e. $150º \leq$ wd $\leq 270º$. The data were roughly classified into three categories: code 1, the M-O theory is valid (no swell, $c_p <$ ws, where $c_p$ and ws are the peak wave and wind speeds, respectively); code 2, the M-

325 O theory is possibly valid (moderate swell, ws $< c_p < 2 \cdot$ws), and code 3, the M-O theory is not valid (dominant swell, $c_p > 2 \cdot$ws). In Fig. 3b the wind speed profiles (cases 1 to 6) are presented in situations where the M-O theory is valid (code 1) and where the M-O theory is not valid (code 3). In Fig. 3c the ambient air temperature profiles are calculated from the same situations as the wind profiles. In Fig. 3d the wind rose at the height of 15.5 m shows the patterns of prevailing wind sectors with wind speed ranges.

330 As an example, Fig. 4a-b depicts the time series of 1-minute-averaged concentrations of the measured gas compounds at 10 m altitude during the first campaign. The sharp peaks in the concentrations of nitrogen monoxide are very striking. In a detailed examination the duration of the emission peaks from the ships were of the order of a few minutes. Where there was a peak in the NO concentration, a negative peak was also detected in the ozone concentration due to the fast reaction producing $NO_2$. This was observed within seconds after the emission from the ship into the atmosphere. The changes in the concentrations

335 of NO, $NO_2$ and $O_3$ were equal, i.e. the change in the concentration of NO took place according to the stoichiometric balance.

The concentration of sulfur dioxide was very low, but clearly distinguishable peaks, with a maximum of 28 ppb, were observed in the data. These peaks originated from the passing ships. The ship peaks were also seen in the $CO_2$ data, but the short-term variation of the $CO_2$ concentration might be larger than the contribution from the ship emissions (Fig. 4b). When looking at the particulate concentrations $N_{tot}$ and $PM_1$ (Fig. 4d), interesting features can be observed. Ship peaks can be clearly

340    distinguished; however, the background levels of $N_{tot}$ and $PM_1$ were highest on 28 August in the morning when the wind blew from the south. The 96 h backward trajectory analysis of Flextra by NILU (Stohl et al., 1995) showed that in the measurement period before the noon of 28 August an air mass was transported through central Europe and arrived in Helsinki (Fig. 5a) carrying anthropogenic pollutants. A sudden drop in the concentrations of $N_{tot}$ and $PM_1$ occurred at noon on 28 August when the wind turned and blew from the west until 10 AM on 30 August (Fig. 4c) over the Altantic and Baltic Sea carrying clean

345    air with low particulate concentrations (Fig. 5b). Simultaneously, the diurnal variation of $CO_2$ diminished. During that period there was no precipitation. During the last 12 hours before the clean air mass arrived in Harmaja the average background particle concentrations stayed rather constant at ~$2.7 \times 10^3$ #/$cm^3$, whereas the $PM_1$ increased from ~ 4 $\mu g/m^3$ to ~ 11 $\mu g/m^3$. This indicates that also larger particles were transported from Europe. In fact, this is obvious from Fig. 6, which presents the average number size distribution (Fig. 6a) as well as the volume size distribution (Fig. 6b) of background particles in the

350    evening of 27 August, at noon on 28 August just before the clean air mass arrived, in the afternoon of 28 August, and early in the morning of 1 September. In the last-mentioned case the particle number concentration was highest ($3.6 \times 10^3$ #/$cm^3$), but due to the small particle sizes (Fig. 6a) they did not have an effect on the volume (and mass) size distribution (Fig. 6b).

### 4.2 Concentration roses

Figure 7 presents the maximum values for the concentrations of each gas compound and the particle number within wind
355    sectors of 10° at both measurement heights. These results are in good agreement with the ones based on the sum of the measured concentrations, thus showing the cumulative contribution from different wind sectors at the measurement point (not shown). For $NO_x$ and $SO_2$, similar patterns were observed indicating the ship routes in sectors 90° to 120°, 150° to 180°, and 270° to 300°. In addition, there is a clear difference in concentrations between the heights: the higher concentrations were mostly at the highest measurement level. In the case of oxygen compounds (= $O_3$ and $O_3+NO_2$) and $CH_4$ the patterns were more evenly
360    distributed. In the case of $CO_2$ and $N_{tot}$ there is an indication of the ship routes, but also of the influence of the city of Helsinki.

### 4.3 Fluxes

Quality control (QC) and quality assurance (QA) procedures are actions that should take into account in order to improve the data quality and to make the data comparable with the similar data from other studies. Although QA and QC procedures have slightly different meanings, in this study, the quality assurance and quality control (QA/QC) procedures are considered
365    together. The following QA/QC procedures and criteria for flux calculations were taken into account.

    1.   Calibration of the used analyzers for gases and particles (Section 3.3), for the GR and EC methods
    2.   Criteria for minimum concentration difference between the measurement heights (Fig. S2), for the GR method

3. Correction of the wind flow field around the measurement mast according to the CFD calculations (Section 4.1), for the GR method

4. Restriction to open sea, i.e. wind direction in the range of 150-270 degrees (Fig. 3a), for the GR and EC methods

5. Analysis of swell to determine the validity of M-O-theory with Codes 1-3 (Section 4.1), for the GR method

6. Footprint area was estimated at each of the measurement height and at neutral, stable and non-stable condition (Fig. 8), for the GR and EC methods

7. Stationarity criteria following the criteria of Foken and Wichura (Foken and Wichura 1998), for the for GR and EC methods

8. The intermittency was applied according to Mahrt et al. (1998), for the EC method

9. WPL correction due to water vapour and heat flux, for the GR and EC methods

10. Cross sensitivity of the compounds on the used analyzers, for the GR and EC methods

11. Preparation of the uncertainty budget for the measurement results, for the GR and EC methods

The footprint area i.e. the area along the upwind where the exchange of gases and particles between the air-sea surface are expected to be a source of the measurement results, was calculated according to Högström et al. (2008). The footprint area was calculated at each of the measured height at stable, neutral and unstable conditions. Fig. 8a illustrates the relative intensity of the footprint area in neutral conditions as a function of upwind distance from the measurement mast at instrument heights of 4.7 m, 7.2 m and 10.7 m. Stable and unstable conditions are presented in Fig. S3. The cumulative relative contribution (Fig. 8b) indicates that at the lowest height (4.7 m) less than 0.3 % of the observed flux takes place at the distance of 20 m from the mast reaching 90 % at a distance of 3 km. At the height of 10.7 m, the footprint area starts at 40 m from the mast reaching 85 % at distance of 3 km. The storage fluxes were not considered in this campaign. The site was by the sea where most of the time the turbulent mixing was most likely the main driving force for gas and particle dispersion.

The stationary requirement was calculated by the method proposed by Foken and Wichura (1996) for fluxes of $CO_2$, momentum, water vapour and heat. Similarly, the effect of flux intermittency was estimated through the index proposed by Mahrt et al (1998).

Cross sensitivity of the compounds (e.g. water vapour) on the response of the used analyzers are included into the uncertainty budget or corrected directly on the results, see in Fig. S1. The influence of NO and $NO_2$ compounds on the response of the $SO_2$-analyzer was tested in the laboratory. Known concentrations of NO and $NO_2$ gases were injected into the $SO_2$-analyzer to define the response function for both NO and $NO_2$. The results of the $SO_2$-analyzer were then corrected accordingly.

The uncertainty sources of the measurement results for fluxes by the gradient method are presented in more detail in Supplementary Table S1. To estimate the uncertainty of the momentum flux and $CO_2$ flux measurements by the EC method we calculated the expected statistical variability using the Co-spectrum. The statistical variability of the covariance (which equals the integral of the Co-spectrum) depends on the shape of the Co-spectrum. A white Co-spectrum implies smaller statistical variability for the covariance than a peaked Co-spectrum. In our estimates we have taken the observed shape of the

$CO_2$ Co-spectrum into account when calculating the estimate of the statistical variability of the covariance, see e.g. Bendat and Piersol, Ch. 7 (2010). For the momentum flux it was 20 %, and for the $CO_2$-flux 30 %. This wide uncertainty range is typical in real meteorological situations and explains the scatter of the EC estimates in e.g. Fig. 12. The analysis of uncertainty follows the guideline provided by the Joint Committee for Guides in Metrology (JCGM, 2008). Based on the analysis, the relative expanded uncertainties for the flux measurements of $CO_2$ and nanoparticles are presented in Table 1 at stationary meteorological conditions.

The eddy diffusivities $K_h$ and $K_m$ describe the conditions of the turbulent mixing for momentum and heat. The latter describes also the behaviour of the gaseous compounds and particles, as explained in section 2.1. In Fig. 9a, the eddy diffusivities $K_h$ and $K_m$ at the measurement level of the sonic anemometer are presented as a function of stability. From Fig. 9a, b, and d, it is also evident that in this data swell occurs mostly in the far unstable conditions, and only in a few cases in stable conditions, while the situations with no swell occur in this data in near the neutral conditions. Wind speed and friction velocity in Fig. 9c show a clear dependence on the wind direction. A linear relationship between the average wind speed and the friction velocity is seen in the sectors where the wind arrives over an open sea area, whereas non-linear behaviour is seen towards the northern sector (345° to 45°), where there are more obstacles. The gradient function in Fig. 9d for momentum has a significant spread around the Businger - Dyer gradient function in the wind sector from 150° to 270°.

Dispersion of a ship plume is schematically presented in Fig. 10a. The black curves denote the edges of the plume. When the lower curve reaches the sea surface the pollutants would be reflected from the sea surface if there were no pollutant flux to the sea. Near the surface the sum of the incident and reflected concentrations will add up to the same value if the reflection is total, thus the forming a new boundary layer where the vertical concentration gradient of the pollutants vanishes. If there is a flux to the sea surface this will result in a vertical gradient of pollutants in this new boundary layer. The fluxes to the sea from the ship can be measured when the plume is over the flux footprint if the measurement instrument is inside the new boundary layer. As an example, Fig. 10b illustrates the momentary plumes at the sea surface for a ship operating to the city of Helsinki and passing Harmaja Island with a speed of 21.5 kn (~11 m s$^{-1}$). The arrows show how the apparent plume is generated in the (u,v)-coordinate system, and where the pollutants advecting to the footprint area come from. In the example the wind speed was 11 m s$^{-1}$ and wind direction 216° as in the afternoon and evening of 28 August (Fig. 4c). The momentary plume figures are shown after 15, 23, 30 and 37 min the start, and the plume concentration gradients decrease as the plume moves further. At the footprint area the gradient is really small indicating horizontally homogeneous situation. If additionally, the stationary criteria for heat, water vapour and momentum are valid, the momentary vertical gradients give the momentary flux.

Before the calculation of fluxes of gases and particles by the GR method, it is necessary to evaluate the measured concentration differences between the measurement heights, with their uncertainty limits. The uncertainty of the gas and particle analyzers as a function of concentration is presented in Supplementary Fig. S1, and the concentration differences between the measurement heights in Fig. S2. Based on the analysis, the concentration differences for $N_{tot}$ exceeded clearly the uncertainty limit enabling the calculation of the $N_{tot}$ fluxes by the GR method. In case of raw $CO_2$, the concentration

difference exceeded the uncertainty limit frequently, but only rarely in case with WPL correction, i.e. in dry air. Consequently, the fluxes for $CO_2$ were too small to be detected by the GR method. On the contrary, the $CO_2$ fluxes obtained by the EC method did not suffer the same problem (direct flux method) and those fluxes were acceptable except in cases when stationary criteria was not fulfilled. We also made the comparison of GR and EC methods with sensible heat (Fig. S4).

440 Clear correlation between the methods can be observed if the calculation of the sensible heat by the GR method was made from the sea surface up the measurement height 11 m and to 15 m. However, the temperature difference between the measurement heights (11 and 15 m) was mostly too small to be detected and no flux could be calculated.

Fig. 11a illustrates the time series for the $CO_2$ flux by the EC method, and Fig. 11b for the $N_{tot}$ flux by the GR method along with the uncertainties. Only the fluxes that fulfilled the stationary criteria with no swell in the wind sector of 150-270

445 degrees were taken into account. For most of the time the $CO_2$ flux was positive (upward) in Fig. 11a, while the flux of $N_{tot}$ was mostly negative (downward) in Fig. 11b. The WPL-correction to the $CO_2$ flux by the EC method corrects wet air into the dry air and for water flux. Due to the damping of temperature fluctuations in the long sample tube the WPL correction for heat flux was insignificant (Rannik et al. 1997). During the period when the air masses were moving from the Atlantic (during 28.8 to 31.8), the correction due to water flux was dominating and caused a positive offset to the $CO_2$ flux (Fig. S5).

450 The observed $CO_2$ fluxes are also in line with the previous measurements (Honkanen et al. 2018) at the Utö island in the Baltic Sea.

Assuming that there is no inversion below the ships' chimneys height, profile measurements of the compounds indicate that the deposition of nanoparticles towards the sea surface is most probably caused by ship emissions (Fig. 11c). More detailed analysis was made to compare the fluxes of $CO_2$ and Ntot calculated from single ship plumes which lasted from 3 to 7 minutes

455 with the 30 min fluxes. Figs. 11c and 11d show clear peaks both in the case of $CO_2$ and nanoparticles, but the contribution of these ship peak fluxes was insignificant compared with the 30 min fluxes (not shown in the figure).

From the campaign in 2012, the $CO_2$ fluxes by the EC methods as measured at Harmaja and on R/V Aranda are presented in Fig. 12a. The corrections to $CO_2$ fluxes measured from humid air samples have been criticized as insufficient (e.g. Landwehr et al. 2014). The fluxes in this study mainly fulfilled the criteria presented in Miller et al. (2010), Sahlée et al.

460 (2011), Blomquist et al. (2014) and Landwehr et al. (2014). The $CO_2$ fluxes measured on R/V Aranda might be underestimated because the flow rate was too small, 10 slpm. No systematic differences were observed when the LI-7200 $CO_2$ fluxes were compared with the LI-7500 on the ship mast and also with the measurements made at Harmaja.

The WPL correction performed to both of the data in 2011 and 2012 was small in general, see Fig S5. In 2011 the sign of the flux was changed after correction of WPL during the period between 28.8. and 31.8. Generally, positive $CO_2$ fluxes

465 are common in winter, and occasionally in summer after the spring algae bloom, since $CO_2$ is less soluble in the warming sea water. In the Baltic Sea, however, the blue-green algae bloom extends the biological active season, and the positive fluxes in coastal regions are mainly caused by frequent upwelling events (e.g. Lehmann and Myrberg, 2008, Norman et al. 2013). The $CO_2$ flux by the EC method and the partial pressure of $CO_2$ in seawater were measured at the same time as the R/V Aranda measurements in late July 2012; the large difference between the partial pressures in the seawater and in the air

470    indicates the upwelling event (Fig. 12c) causing the positive $CO_2$ fluxes in Fig. 12a. The scatter plot of the $CO_2$ fluxes at Harmaja and on R/V Aranda is presented in Fig. 12b. The large scatter is most probably due to the different locations: the measurements of $pCO_2$ (Fig. 12c) suggest that the $pCO_2$ was not spatially homogeneous. The estimated statistical variability is large and also contributes to the scatter. The sensible heat fluxes (Fig. 12d) were calculated by the EC method in 2012 campaign at Harmaja and at two heights (10 m and 16 m above the sea level) at R/V Aranda showing good agreement with

475    each other.

       Unfortunately, direct comparison between the $CO_2$ fluxes by the EC and GR methods in Harmaja in 2011 as well as in 2012 at R/V Aranda could not be performed due to the fact that the $CO_2$ fluxes were too small to be detected by the GR method. Discrepancies between the measurement results by the GR and EC methods have been reported in the literature (Mycklebust et al. 2008, Muller et al. 2009) for $CO_2$ and for $O_3$, but no systematic reason has been found.

480

### 4.4 Fuel sulphur content

       The FSC was determined in the measurement campaigns in both 2011 and 2012. The two campaigns differed from each other in the measurement strategies, but also in the data collecting frequency, once a minute in 2011 and every 15 s in 2012. In both cases, the data acquisition system calculated the averages over the data collecting time. It became very clear that the frequency

485    of once a minute was too low in order to see accurate emission peaks in the ship plumes, because the duration of the plume itself was of the order of a few minutes. This was the reason for shortening the response time of the analyzers by increasing the flow rate from the nominal flow and shortening the integration time, which then made it possible to increase the data collecting frequency.

       As seen from Supplementary Fig. S6, major factors influencing the accuracy of calculating the emission peak area are the

490    difference of the response time between the $SO_2$ and $CO_2$ analyzers, but also the frequency of data collection. The Picarro G2301 $CO_2$ analyzer is clearly faster than the UV-Fluorescence $SO_2$ analyzers, which are designed for air quality measurements to meet the requirements of EU regulations. Even when improvements were made to the $SO_2$ analyzer between the 2011 and 2012 campaigns, the difference in the peak width is clearly seen.

       The variation between the 2011 and 2012 campaigns in the calculated FSC from the ships that routinely cruise between

495    Helsinki and Stockholm or Helsinki and Tallinn is used when estimating the uncertainty of the FSC according to Eq. (13). In Fig. 13 the relative expanded uncertainty for the FSC, $U_{FSC}$ (%), is shown as a function of peak height concentration of $SO_2$. Calculation of $U_{FSC}$ (%) was made for FSC = 0.1 %, 0.5 % and 1 % fulfilling the requirement according to the regulation at the time of the measurements (FSC = 1 %) but also the regulation which came into power in 2014 (Directive, 2012/33/EU) for SECA areas (FSC = 0.1 %) and for oceans (FSC = 0.5%). The uncertainty of the FSC increases rapidly, being 100 % at a peak

500    concentration of 3 ppb for a FSC of 0.1 %, and 5 ppb for a FSC of 0.5 %. When more accurate measurements are required, the peak height concentration of $SO_2$ should be clearly higher than 5 ppb or 10 ppb for the FSC regulation of 0.1 % or 0.5 %, respectively. Considering that the highest peak concentration observed was 50 ppb which gives the uncertainty of 18 % for

FSC. At the same time the NO peak was 100 ppb giving a response to SO2 analyzer of 2 ppb or 4 % of the measured $SO_2$ with the cross sensitivity of 2 %. According to the present regulation, FSC = 0.1% similarly, the highest peak concentration would be 5 ppb of SO2 with the uncertainty of 25 %. The NO would still be 100 ppb giving respond of 2 ppb on the $SO_2$ results being 40 % of the measured SO2 concentration. Correction of the cross sensitivity for nitrogen compounds on the response of SO2 analyzer by UV fluorescence technique is vital.

No violation against the regulation was observed for the calculated FSC during the campaigns in 2011 and 2012 (Fig. 14). A typical value for FSC 0.4 % was obtained at an uncertainty of 15 % i.e. $0.40 \pm 0.06$ %. Also the obtained FSCs were in good agreement with the information given by the ship owners, as well with our earlier results in Pirjola et al. (2014), where emissions from the same ships were studied in winter and summer campaigns in 2010 and 2011. The mobile laboratory Sniffer was standing at the harbour areas in Helsinki and Turku. Besides the FSCs we also estimated the emissions factors for NO, $NO_x$, $SO_2$, Ntot and $PM_{2.5}$, For example, the emission factors for NOx were in the range of 56 to 100 g $(kg\ fuel)^{-1}$.

## 5 Conclusions

Direct exchange of gaseous compounds and nanoparticles between air and sea interface was studied by micrometeorological methods. The gas compounds $SO_2$, NO, $NO_2$, $O_3$, and $CO_2$, as well as the number concentration of nanoparticles, $N_{tot}$, were measured at the Baltic Sea beside the major ship routes to and from the City of Helsinki. Flux measurements in marine environment are challenging due to meteorological conditions and topographical aspects. Filtering of data outside the footprint area and for certain wind sector, occurrence of swell, non-stationarity, and the concentration difference between the measurement heights less than the uncertainty limit reduces the number of available data considerably. In this study, fluxes of 43 % for $N_{tot}$ by the GR method and 28 % for $CO_2$ by the EC method of all measurement results were acceptable.

It became quite clear that no direct gas exchange across the air-sea interface, negative or positive fluxes, could be measured by the GR method. Mostly because the capability of the used analyzers to measure the gas concentration differences under clean coastal conditions was not sufficient. Even though the $CO_2$ flux was too small to be detected with the GR method, it could be detected by the EC method. The case was different for nanoparticles where the observed differences of the number concentration were well above the uncertainty limit for the both ELPIs.

Both of the GR and EC methods were capable for measuring the emissions from the ships. Much effort was laid down on studying the transport and dispersion of single ship emissions. Different scenarios depending on the wind speed and wind direction were able to identify: (i) pollutants have reached the footprint area and the measurement mast (ii) the pollutants bypass the footprint area but are seen by the measurement mast. When the mixing of the pollutants occurred well before the footprint area for the measurement mast the measured fluxes were real. When the mixing of the pollutants from the ships was not complete, violation of the M-O theory occurred and the measurement results described dispersion of the pollutants

The measurements for determining the FSC were in good agreement with the information given by the ship owners. The measurement method used to determine the FSC content of marine fuel from the ambient air in connection with the identification data from AIS gives a clear demonstration of whether the regulations are respected.

The uncertainty analysis of the fluxes and the FSC was conducted according to the well-known law of propagation of errors, and following the recipes from the literature (JCGM, 2008). The uncertainty budget, pointing out the sources of uncertainties and their contribution on the measurement results, may be conservative, but it can be made more accurate on the selecting better measurement technique, capabilities of the analyzers, measurement site and meteorological situations.

To improve the accuracy for determining the FSC based on measurements of the ratio of $SO_2$ to $CO_2$ from emission peaks of ship plumes, development of an instrumentation that can simultaneously measure $SO_2$ and $CO_2$ concentration fast enough and with the same order of response time is highly desirable.

*Data availability*. The data used in this study are available upon request from the corresponding author.

*Supplement*. The supplement related to this article is available online.

*Author contributions.* JW and LP designed the concept of the study. JW, LP, TW performed the measurements with the help of TL, JH, TT and MM. HP and KK were responsible for the Aranda measurements and the aspects in the marine boundary layer. HN carried out the OpenForm simulations, J.-PJ provided the AIS data and NOx emissions from ships (Fig. 1). JW wrote the original manuscript, LP, HP, KK, J.-P.J edited. All authors have read and agreed to the published version of the manuscript.

*Competing interests.* The authors declare that they have no conflict of interest.

*Acknowledgements.*The measurements were carried out during the SNOOP project, financed by the Cental Baltic INTERREG IV A Programme 2007–2013 and the Centre for Economic Development, Transport and the Environment (ELY) of Southwest Finland. This project has also received funding from the European Union's Horizon 2020 research and innovation programme under grant agreement #814893 (SCIPPER project). This work reflects only the authors' view and INEA is not responsible for any use that may be made of the information it contains. The authors are very grateful to Mr. Aleksi Malinen at Metropolia University of Applied Sciences for help in the measurements and to Ms. Kaisa Lusa and Sisko Laurila at the Finnish Meteorological Institute for help in laboratory calibrations. For revision of the language, the authors are very grateful to Ms. Leena Kahma. Editor and anonymous Referees are thanked for their critical and insightful but constructive comments improving considerably the final manuscript.

**References**

Alföldy, B., Lööv, J. B., Lagler, F., Mellqvist, J., Berg, N., Beecken, J., Weststrate, H., Duyzer, J., Bencs, L., Horemans, B., Cavalli, F., Putaud, J.-P., Janssens-Maenhout, G., Csordás, A. P., Van Grieken, R., Borowiak, A., and Hjorth, J.: Measurements of air pollution emission factors for marine transportation in SECA, Atmos. Meas. Tech., 6, 1777–1791, doi:10.5194/amt-6-

570    1777-2013, 2013

Bendat, J.S. and Piersol, A.G.:  Random Data; Analysis and Measurement Procedures. (4th ed.). John Wiley and Sons, New York, 2010.

Blomquist B. W., Huebert, B. J., Fairall, C. W., Bariteau, L., Edson, J. B., Hare, J. E., McGillis, W. R.: Advances in Air-Sea $CO_2$ Flux Measurement by Eddy Correlation, Boundary-Layer Meteorol. 152,245-276. DOI 10.1007/s10546-014-9926-2,

575    2014

Businger, J.A.: Evaluation of the Accuracy with Which Dry Deposition Can Be Measured with Current Micrometeorological Techniques, J. Climate and Appl. Meteorol., 25, 1100 - 1124, 1986.

Businger, J. A., Wyngaard, J. C., Izumi, Y., and Bradley, E.F.: Flux profile relationships in the atmospheric surface layer, J. Atmos. Sci., 28, 181 -189, 1971.

580    Cooper, D. A.: HCB, PCB, PCDD and PCDF emissions from ships, Atmos. Environ., 39, 4901–4912, 2005.

De Leeuw G., Ambelas Skjøth C., Hertel O., Jickells T., Spokes L., Vignati E., Frohn L., Frydendall J., Schulz M., Tamm S., Sørensen L.L., Kunz G.J. Deposition of nitrogen into the North Sea. Atm, Env. 37 Supplement No1, S145 – S165, 2003.

Directive 1999/32/EC. Sulphur content in Marine fuels.

Directive 2012/33/EU. Sulphur content in Marine fuels.

585    Drennan, W., Donelan, M. A., Madsen, N., Katsaros, K. B., Terray, E., Flagg, C. N.: Directional Wave Spectra from a Swath Ship at Sea, J. Atmos. Ocean. Technol., 11, 896-908, DOI: 10.1175/1520-0426(1994)011<1109:DWSFAS>2.0.CO;2, 1994.

Drennan, W. M., Graber, H. C., Hauser, D., Quentin, C.: On the wave age dependence of wind stress over pure wind seas, J. Geophys. Res., 108, 8062,8075, doi 1029/2000JC000715, 2003.

Dyer, A. J.: A review of flux-profile relations, Boundary Layer Meteorol., 1, 363 – 371, 1974.

590    Dyer, A. J., Hicks, B. B.: Flux-gradient relationships in the constant flux layer. Quart. J. R. Met. Soc. 96, 715-721, 1970.

Duyzer, J. H., Deinum, G., Baak, J.: The interpretation of measurements of surface exchange of nitrogen oxides: correction for chemical reactions, Phil. Trans. R. Soc. Lond. 351, 231 – 248, 1995.

Foken, T, Wichura, B. Tools for quality assessment of surface-based flux measurements. Agric. Forest Meteorol. 78, 83 – 105, 1996.

595    Haerri, H.-P.,  Macé, T., Waldén, J., Pascale, C., Niederhauser,  B., Wirtz, K., Stovcik, V., Sutour, C., Couette, J., Waldén T.: Dilution and permeation methods for the generation of NO, $NO_2$ and $SO_2$ calibration gas mixture,  Meas. Sci. Technol., 28, 035801, DOI: 10.1088/1361-6501/aa543d, 2017.

HELCOM Maritime19/5-2.INF "Emissions from Baltic Sea shipping in 2006 – 2018", by Jalkanen, J.-P. and Johansson L: https://portal.helcom.fi/meetings/MARITIME%2019-2019-582/MeetingDocuments/5-

600   2%20Emissions%20from%20Baltic%20Sea%20shipping%20in%202006%20-%202018.pdf, last access 4.4.2020.

Hongisto, M. and Joffre, S.: Meteorological and climatological factors affecting transport and deposition of nitrogen compounds over the Baltic Sea, Boreal Env. Res., 10, 1–17, 2005.

Hongisto, M.: Impact of the emissions of international sea traffic on airborne deposition to the Baltic Sea and concentrations at the coastline, Oceanologia, 56, 349-372, 2014.

605   Honkanen M., Tuovinen J-P., Laurila T., Mäkelä T., Hatakka J., Kielosto S., Laakso L. Measuring turbulent $CO_2$ fluxes with closed-path gas analyzer in marine environment. Atmos. Meas. Tech. 11, 5335 – 5350, 2018.

Högström, U., Sahlée, E., Drennan, W. M, Kahma, K. K., Smedman, A.-S., Johansson, C., Pettersson, H., Rutgersson A., Tuomi, L., Zhang, F., Johansson, M.: Momentum fluxes and wind gradients in marine boundary layer – a multi-platform study, Boreal Env. Res., 13, 475-502, 2008.

610   Högström, U., Rutgersson, A., Sahlée, E., Smedman, A.-S., Hristor, T., S., Drennan, W. M., Kahma, K. K.; Air-sea interaction features in the Baltic Sea and at a Pacific trade-wind site: an Inter-comparison study, Boundary-Layer Meteorol, 147, 139-163, DOI 10,1007/s10546-012-9776-8, 2013.

Högström, U., Sahlée, E., Smedman, A.-S., Rutgersson, A., Nilsson, E., Kahma, K.K., Drennan, W. M. J., Surface Stress over the Ocean in Swell-Dominated Conditions during Moderate Winds, J. Atmos. Sci., 72, 4777–4795, 2015, DOI: 10.1175/JAS-

615   D-15-0139.1.

IMO: International Maritime Organisation, Guidelines for the Control and Management of Ships' Ballast Water to Minimise the Transfer of Harmful Aquatic Organisms and Pathogens, http://www.imo.org/en/KnowledgeCentre/IndexofIMOResolutions/Assembly/Documents/A.868%2820%29.pdf, last access 17.9.2020.

620   JCGM; Evaluation of measurement data – Guide to the expression of uncertainty in measurement, JCGM, 100, 2008.

Jalkanen, J.-P., Brink, A., Kalli, J., Pettersson, H., Kukkonen, J., and Stipa, T.: A modelling system for the exhaust emissions of marine traffic and its application in the Baltic Sea area, Atmos. Chem. Phys., 9, 9209-9223, 2009.

Johansson, L., Jalkanen, J.-P.: Emissions from Baltic Sea Shipping in 2015, https://helcom.fi/baltic-sea-trends/environment-fact-sheets/maritime-activities/emissions-from-baltic-sea-shipping-in-2015/, 2016, last access 17.9.2020.

625   Johnsson J.E., Gauss M., Schulz M., Jalkanen J.-P., and Hagerli H.: Effects of global ship emissions on European air pollution levels. Atmos.Chem.Phys., 20, 11399 – 11422, 2020.

Kahma, K, K., Donelan, M. A., Drenman, W. M., Terray, E. A.: Evidence of energy and momentum flux from swell to wind, J. Phys. Oceanogr, 46, 2143-2156, https://doi.org/10.1175/JPO-D-15-0213.1, 2016.

Kaimal, J.C., Finnigan J. J.: Atmospheric boundary layer flows: their structure and measurement, Oxford University Press,

630   New York, 1994.

Keskinen, J., Pietarinen, K., Lehtimäki, M.: Electrical low pressure impactor, J. Aerosol Sci., 23, 353-360, 1992.

Kramm, G., Müller, H., Fowler, D., Höfken, K.D., Meixner, F.X., Schaller, E.: A modified Profile Method for Determining the Vertical Fluxes of NO, $NO_2$, Ozone and $HNO_3$ in the Atmospheric Surface Layer, Journal of Atmospheric Chemistry, 13, 265 – 288, 1991.

635 Landwehr, S., Miller, S. D., Smith, M. J., Saltzman, E. S., Ward, B.: Analysis of the PKT correction for direct $CO_2$ flux measurements over the ocean, Atmos. Chem. Phys. 14, 3361-3372. doi:10.5194/acp-14-3361-2014, 2014.

Lehmann, A., Myrberg, K.: Upwelling in the Baltic Sea - a review, Phys. Chem. Earth, B 25, 183-189, 2008.

Lenschow, D. H., Kristensen, L.: Uncorrelated noise in turbulence measurements, J. Atmos. Ocean. Tech., 2, 68–81, 1985.

Lenschow, D., Delany, A. C.: An analytical Formulation for NO and $NO_2$ Flux Profiles in the Atmospheric surface Layer,

640 Journal of Atmospheric Chemistry, 5, 301 – 309, 1987.

Lenschow, D. H., Mann, J., Kristensen, L.: How long is long enough when measuring fluxes and other turbulence statistics?, J. Atmos. Ocean. Tech., 18, 661–673, 1994.

Mahrt, L., Sun, J., Blumen, W., Delany, A.C, Oncley S. Nocturnal Boundary-Layer Regimes. Boundary-Layer Meteorology 88, 255 – 278, 1998.

645 Marjamaki, M., Ntziachristos, L., Virtanen, A., Ristimäki, J., Keskinen, J., Moisio, M., Palonen, M., Lappi, M.: Electrical Filter Stage for the ELPI. Society of Automotive Engineers, SAE Technical Paper 2002-01-0055, 2002.

Mellquist, J., Beecken, J., Conde, V., Ekholm, J.: Surveillance of Sulfur Emissions from Ships in Danish Waters, Final Report to Danish Environmental Agency, DOI: 10.17196/DEPA.001,2018.

Miller, S. D., Maradino, C., Saltzman, E. S.: Ship-based measurement of air-sea CO2 exchange by eddy covariance – J.

650 Geophys. Res. 115, D02304, doi:10.1029/2009JD012193, 2010. Moldanová, J., Fridell, E., Winnes, H., Holmin-Fridell, S., Boman, J., Jedynska, A., Tishkova, V., Demirdjian, B., Joulie, S., Bladt, H., Ivleva, N. P., and Niessner, R.: Physical and chemical characterization of PM emissions from two ships operating in European Emission Control Areas, Atmos. Meas. Tech. Discuss., 6, 3931– 3982, doi:10.5194/amtd-6-3931-2013, 2013.

Muller J. B. A., Coyle M., Fowler D., Gallagher M., Nemitz E. G., Persival C. J. Comparison of ozone fluxes over grassland

655 by gradient and eddy covariance technique. Atmos. Sci. let. 10, 164 – 169, 2009.

Myklebust M. C., Hipps L. E., Ryel R. J. Comparison of eddy covariance, chamber, and gradient methods of measuring soil CO2 efflux in an annual semi-arid grass, Bromus tectorum. Agric. For. Meteorol. 148, 1894 – 1907, 2008.

Norman, M., Parampil, S. R., Rutgersson, A, Sahlée, E.: Influence of coastal upwelling on the air-sea gas exchange of $CO_2$ in a Baltic Sea Basin, Tellus B, 65, 21831, http://dx.doi.org/10.3402/tellusb.v65i0.21831, 2013.

660 OpenFOAM: http//www.openfoam.org, 2020, last access 7.4.2020.

Panofsky, H. A., Dutton, J. A.: Atmospheric turbulence - Models and methods for engineering applications. John Wiley & Sons, Inc., New York, USA, 397 p, 1987.

Paulson, C. A.: The Mathematical Representation of Wind Speed and Temperature Profiles in the Unstable Atmospheric Surface Layer, J. Appl. Meteor., 9, 857-861, 1970.

665    Petzold, A., Hasselbach, J., Lauer, P., Baumann, R., Franke, K., Gurk, C., Schlager, H., Weingartner, E.: Experimental studies on particle emissions from cruising ship, their characteristic properties, transformation and atmospheric lifetime in the marine boundary layer, Atmos. Chem. Phys., 8, 2387–2403, doi:10.5194/acp-8-2387-2008, 2008.

Pirjola L., Pajunoja A., Walden J., Jalkanen J.-P., Rönkkö T., Kousa A., Koskentalo T.: Mobile measurements of ship emissions in two harbour areas in Finland, Atmos. Meas. Tech., 7, 149 – 161, 2014.

670    Rannik, U., Vesala, T., and Keskinen, R. On the damping of temperature fluctuations in a circular tube relevant to the eddy covariance measurement technique. J. Geophys. Res. 102, 12789 – 12794, 1997.

Rannik, Ü., Kolari, P., Vesala, T., Hari, P.: Uncertainties in measurement and modelling of net ecosystem exchange of a forest ecosystem at different time scales, Agr. Forest Meteorol., 138, 244–257, 2006.

Rinne, J. Tuovinen J.-P., Laurila, T., Hakola, H., Aurela, M., Hypen, H.: Measurements of hydrocarbon fluxes by a gradient
675    method above a northern boreal forest, Agricultural and forest meteorology, 102, 25 – 37, 2000.

Seinfeld, J. H., Pandis, S. N.; Atmospheric Chemistry and Physics: From Air Pollution to Climate Change, Wiley, 2012.

Sahlée, E., Kahma, K., Pettersson, H., Drennan, W. M.: Damping of humidity fluctuations in a closed-path system.- In In Gas Transfer at Water Surfaces 6 (Eds. Komori S., McGillis W. and Kurose R.), Kyoto University Press, Kyoto, Japan, 516-523, 2011.

680    Seppälä S., Kuula J., Hyvärinen A.-P., Saarikoski S., Rönkö T., Keskinen J., Jalkanen J.-P., Timonen H.: Effects of marine fuel sulfur restrictions on particle number concentrations and size distributions in ship plumes at the Baltic sea. https://doi.org/10.5194/acp-2020-949.

Smedman, A., Högström, U., Bergström, H., Rutgersson, A., Kahma, K. K., Pettersson H.: A case-study of air-sea interaction during swell conditions, J. Geophys. Res., 104, 25833 – 25851, 1999.

685    Stohl, A., Wotawa, G., Seibert, P., Kromp-Kolb, H.: Interpolation errors in wind fields as a function of spatial and temporal resolution and their impact on different types of kinematic trajectories, J. Appl. Meteor., 34, 2149-2165, 1995.

Webb, E.K., Pearman, G. I., Leuning R.: Correction of flux measurements for density effects due to heat and water vapour transfer, Quart. J. Met. Soc., 106, 85 – 100, 1980.

Vila-Guerau de Arellano, J., Duynkerke, P. G., Builtjes, P. J. H.: The divergence of the turbulent diffusion flux in the surface
690    layer due to chemical reactions: the NO-O$_3$-NO$_2$ system, Tellus, 45B, 23 – 33, 1993.

Williams, E. J., Lerner, B. M., Murphy, P. C., Herndon, S. C., Zahniser, M. S.: Emissions of NOx, SO2, CO and HCHO from commercial marine shipping during Texas Air Quality Study (TexAQS) 2006, J. Geophys. Res., 114, D21306, doi:10.1029/2009JD012094, 20

WMO 2013. WMO/IAEA Meeting on Carbon Dioxide, Other Greenhouse Gases and Related Tracers Measurement
695    Techniques GGMT-2013, GAW report 213, July 2014.

Yli-Ojanperä, J., Kannosto, J., Marjamäki, M., Keskinen, J.: Improving the nanoparticle resolution of the ELPI, Aerosol. Air Qual. Res., 10, 360–366, 2010.

700  Table 1. Estimated relative expanded uncertainties for the fluxes of gaseous $CO_2$ and nanoparticles by the GR method, and for $CO_2$ by the EC method in meteorological situations of stationary ($U_{Stat.Met.}$). More details of the uncertainty budget are presented in Supplementary Table S1. The uncertainty values are given at the median flux values.

| Flux | Method | Flux (median) | | $U_{Stat.Met.}$ |
|------|--------|---------------|---|-----------------|
| $F_{CO2}$ | EC | -0.081 | $\mu mol\ m^{-2}\ s^{-1}$ | 30.0 % |
| $F_{Ntot}$ | GR | -229.1 | $cm^{-3}\ m\ s^{-1}$ | 30.8 % |
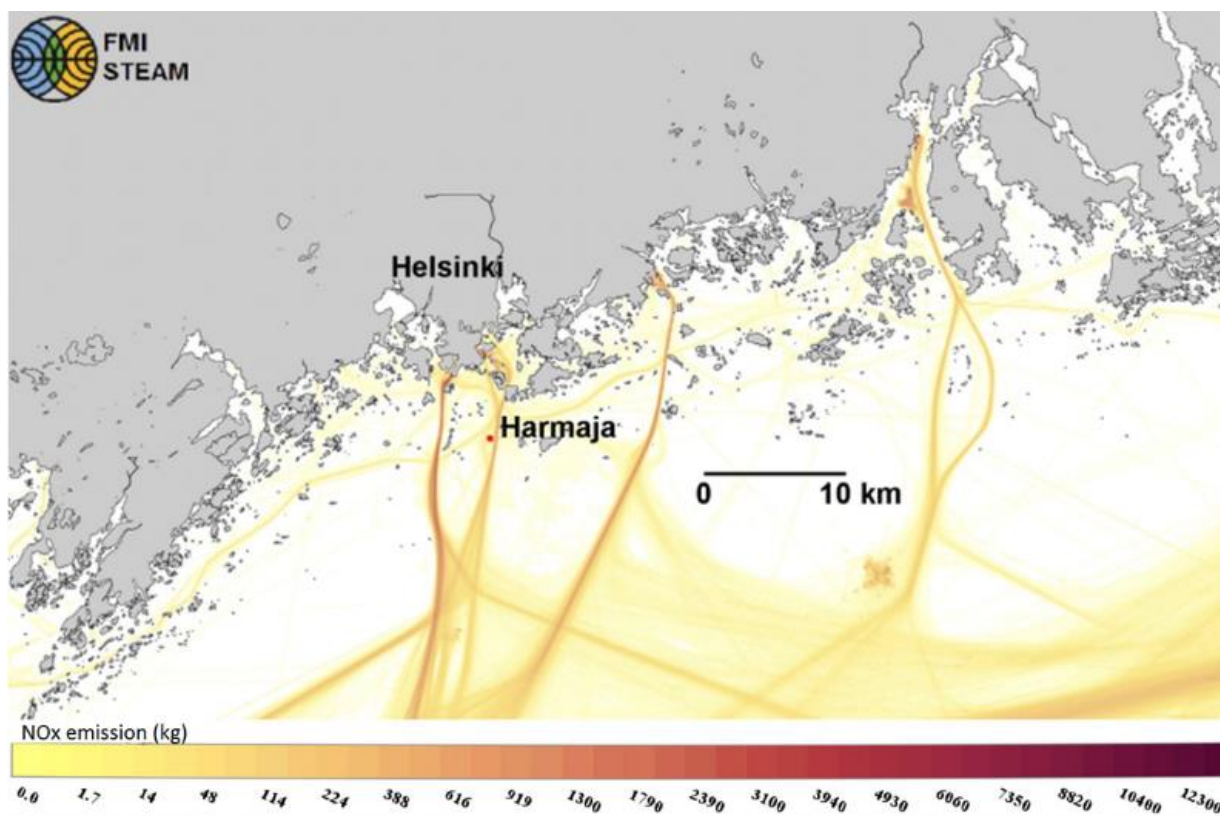
Figure 1. International ship routes at the Baltic Sea and the ship routes to the harbors of Helsinki along with the modelled NOx emissions. Land area is marked by grey, sea by white, and NOx emissions in kg by color indicated on the bar. Harmaja Island is marked by a red circle.

710
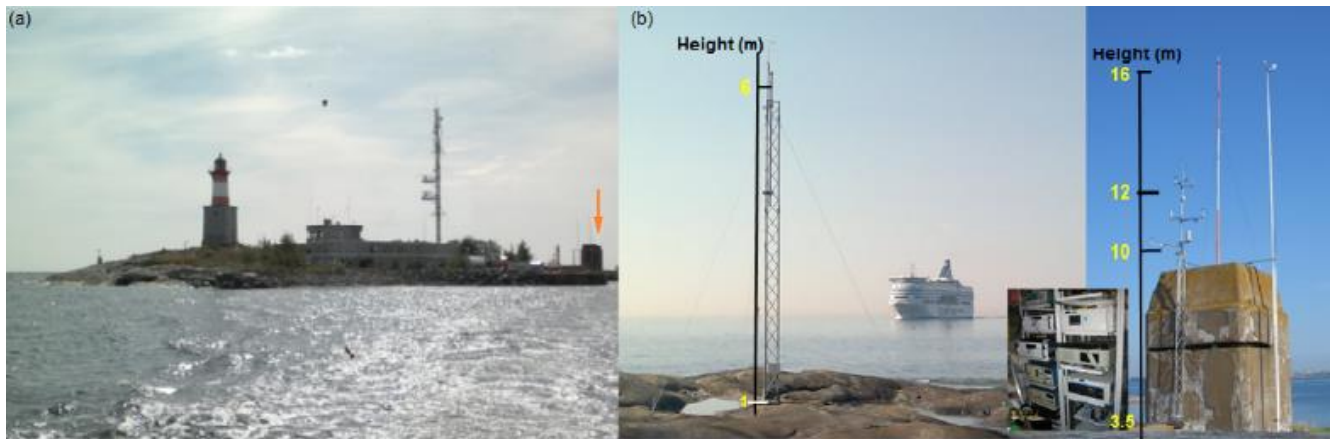
715    Figure 2. a) Harmaja island. The red arrow points to the measurement tower. b) Measurement instrumentation was installed in racks inside the fire control tower. The mast on the right includes all the measurement probes (wind and temperature probes and sample intakes) for the gradient and eddy covariance methods during the 2011 campaign, whereas the mast on the left includes the probes and sample inputs for the eddy covariance method and for measuring gas and particle concentration during the 2012 campaign. Both masts faced the open sea. The masts stood approximately 20 m from the shoreline and 3.5 m above MSL in 2011, and 3 m from the shoreline and 1 m above MSL in 2012.

720    The official weather mast of the FMI is located by the side of the tower (right-side mast, 16.6 m).

a)
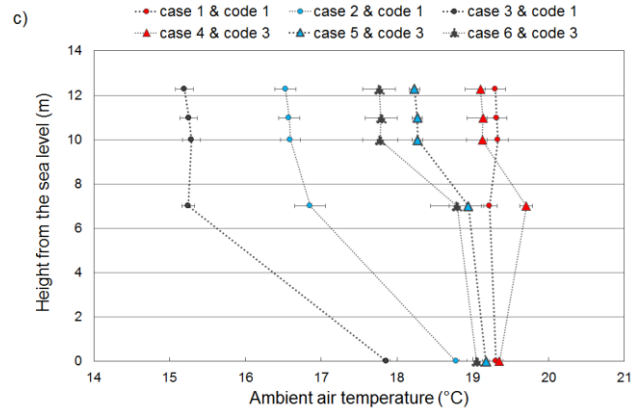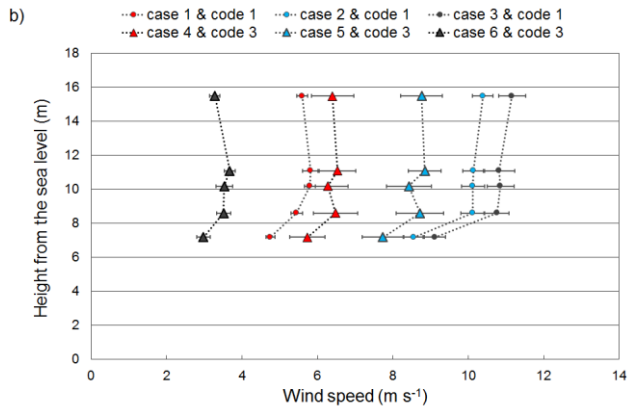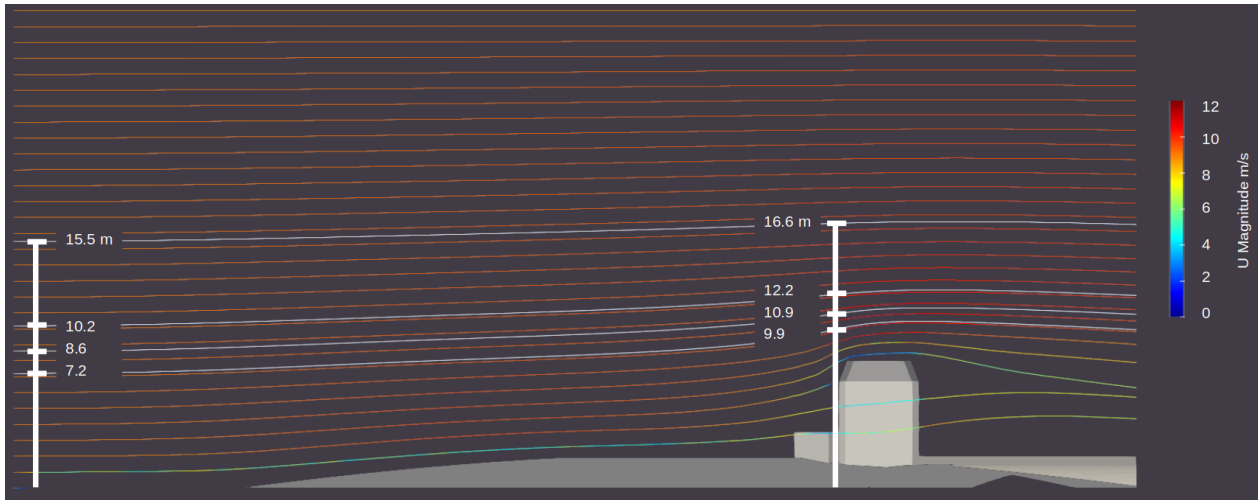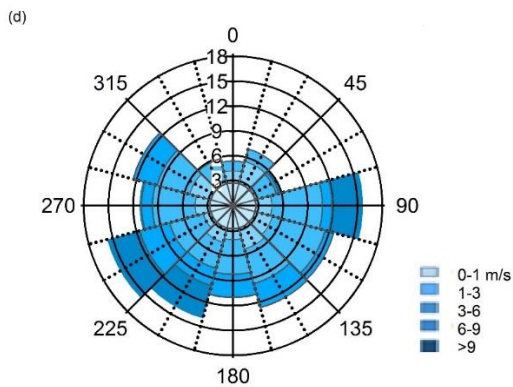
Figure 3. a) The actual measurement heights were reduced to corresponding heights over the open sea surface utilizing calculated isopleths from flow dynamics program. The actual wind speed probe heights at the measurement mast are shown on the right and their projected

heights over open sea on the left.  b) Mean wind speed profiles over 2 to 3 hours are presented at different heights in the wind direction

730     sector from $150^o$ to $270^o$. The dots represent the situations of no swell (code 1), while the squares represent cases of swell (code 3). The

error bars show the standard deviation of the wind speed over the average period at the respective heights. c) Hourly mean temperature

profiles are presented from the same situations as the wind profiles in Fig**.** 3b. The error bars show the standard deviation of the

temperature over the average period at the respective heights. d) Wind rose of direction (scale as %) and wind speed (m/s) at different

ranges at the measurement height of 16.6 m.

735
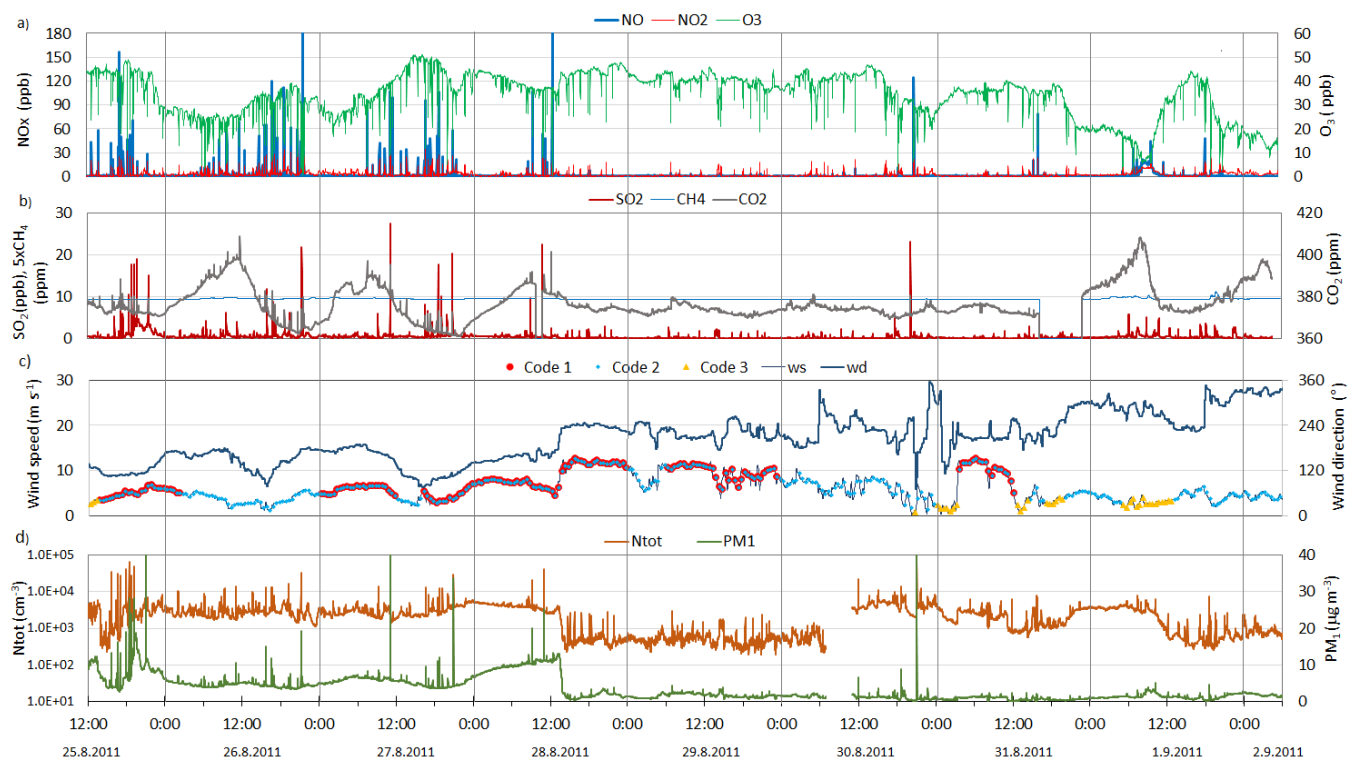
Figure 4. Time series of one-minute average concentrations of gaseous (a-b) and particulate matter (d) as well as the wind speed and wind direction (c) during 25.8.-2.9.2011. Also shown in c) are the 30 minutes average wind speed in different situations regarding the M-O theory, i.e. codes 1 to 3.

740
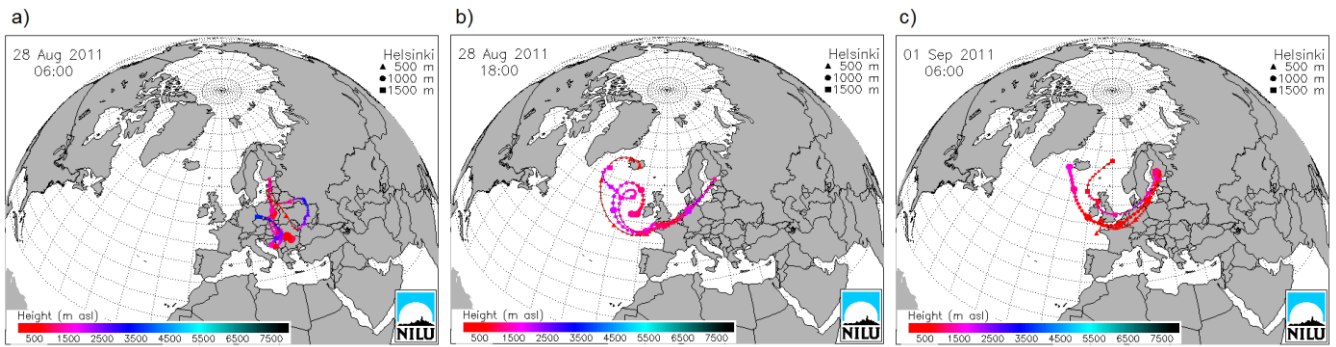
Figure 5. Selected airmass trajectories 28.8. at 6 am (a) and at 6 pm (b), and 1.9. at 6 am (c) during our campaign of 2011. The times are given in UTC, whereas our data sets are given in EET (UTC+2).
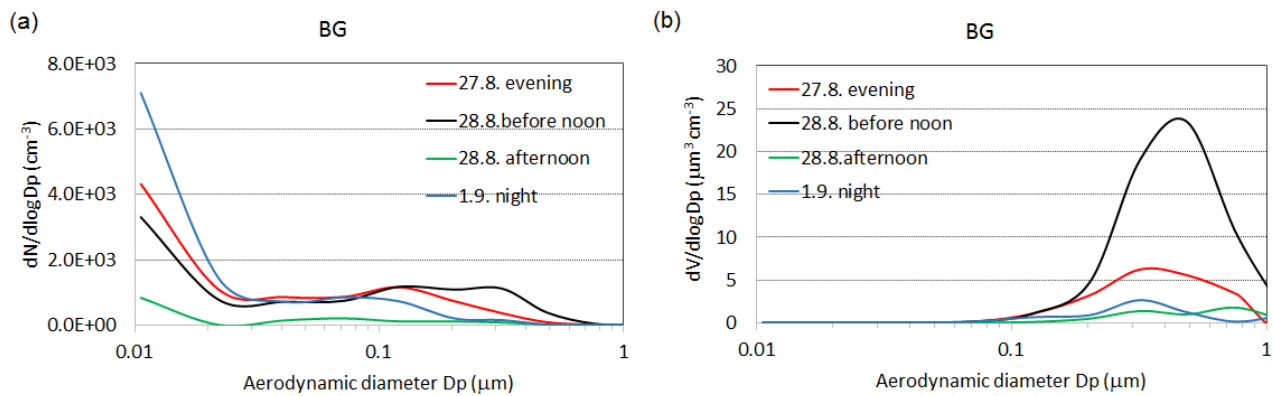
750    Figure 6. Number (a) and volume (b) size distributions of background particles.
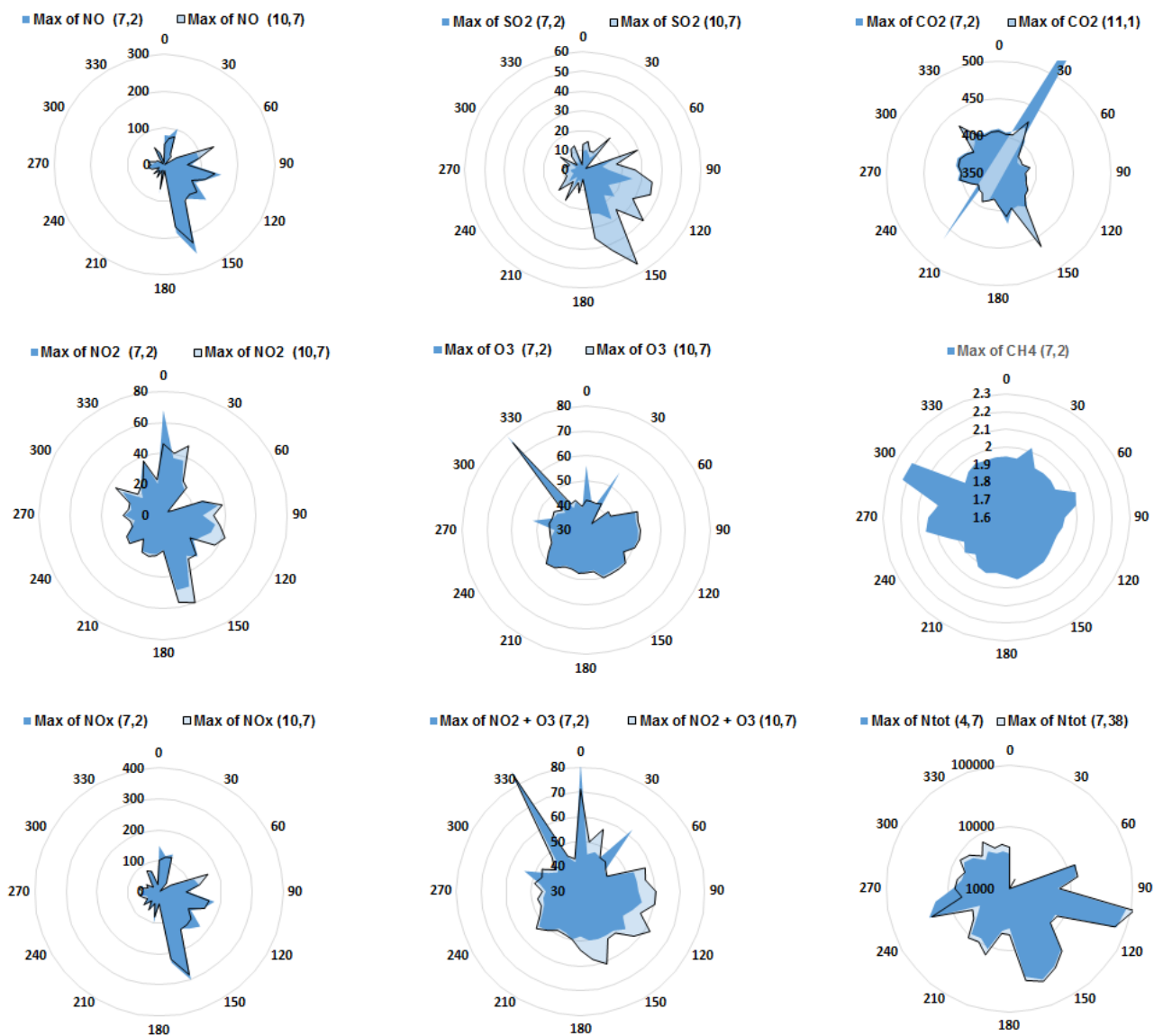
Figure 7. Roses of the maximum gaseous concentrations of nitrogen oxides (NO, NO₂, NOₓ) in ppb, oxidants O₃ and NO₂+O₃, as well as SO₂ in ppb, and CH₄ and CO₂ in ppm. Also shown are the roses of particle concentrations $N_{tot}$ in #/cm³. All roses, except for CH₄, were plotted from the two heights; the corrected heights (m) are given in parentheses above the roses. The direction of the coastline is from 240 to 60 degrees.
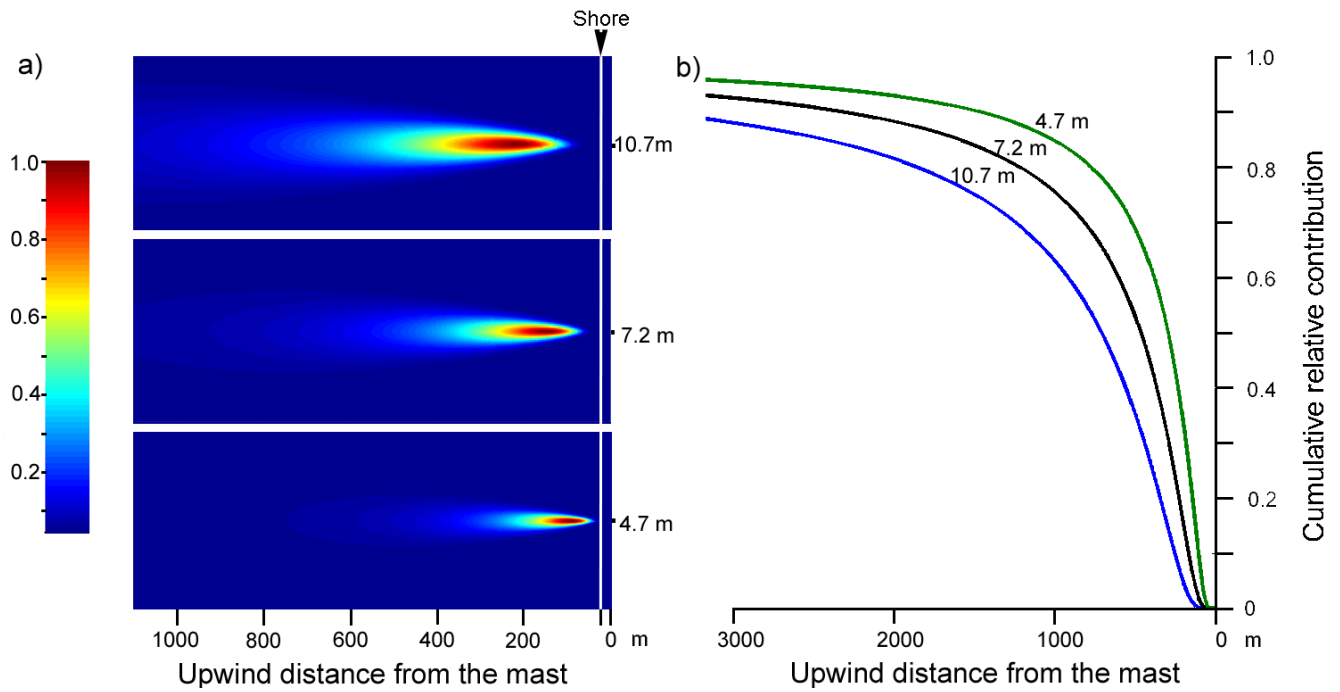
Figure 8. a) Flux footprint areas at neutral stability seen by the $CO_2$ instruments at 10.7 and 7.2 altitudes, and by the ELPIs at 7.2 and 4.7 m
765   altitudes, as recalculated in Fig. 3a. X-axis refers to the upwind distance from the instruments, and the colour bar to the relative intensity of
the sea surface area to the flux. Figure b) shows the cumulative relative contribution.

770
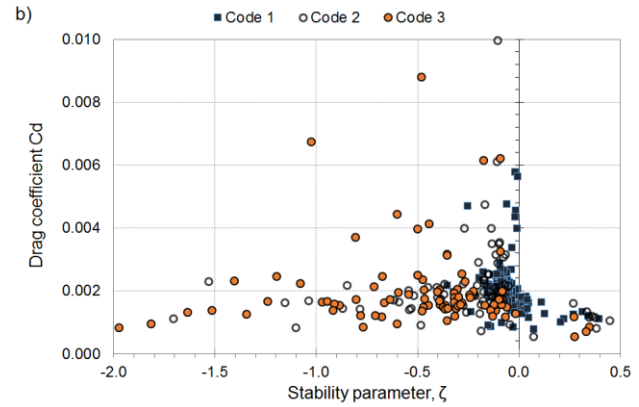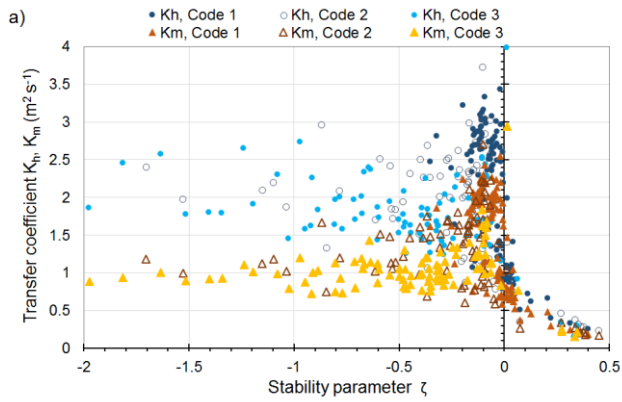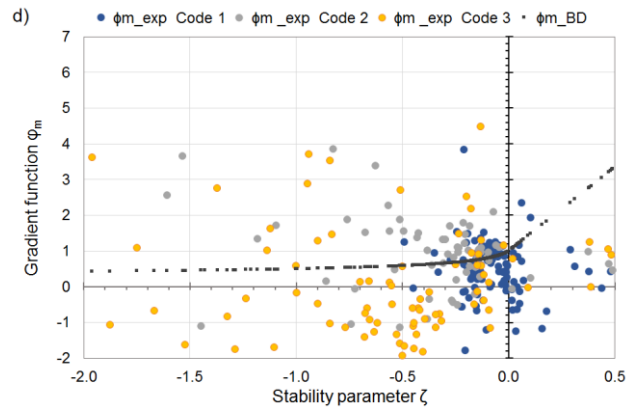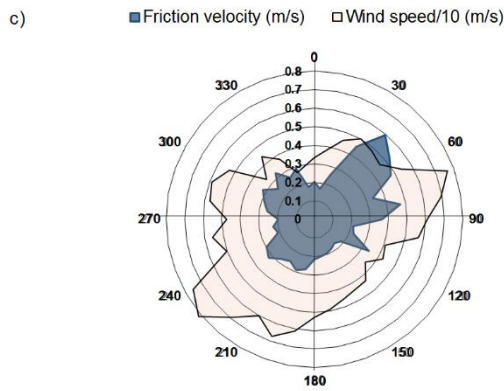
Figure 9. a) The eddy diffusivity coefficients $K_{h,}$(blue) and $K_m$ (brown) as a function of stability at height 12.28 m and with wave codes 1, 2

775    and 3. b) The friction velocity by sonic anemometer as a function of stability at 11.1 m height with wave codes 1, 2 and 3. c) The rose of

friction velocity and wind speed (divided by 10) as averages over the wind sectors of 10°. d) The gradient functions from the experiments

($\phi_m$_exp) at the 15.5 m altitude and from the Businger - Dyer formula ($\phi_m$_BD). In a), b), and d) the stationary criteria in wind sector 150-

270 ° is based on the momentum flux.
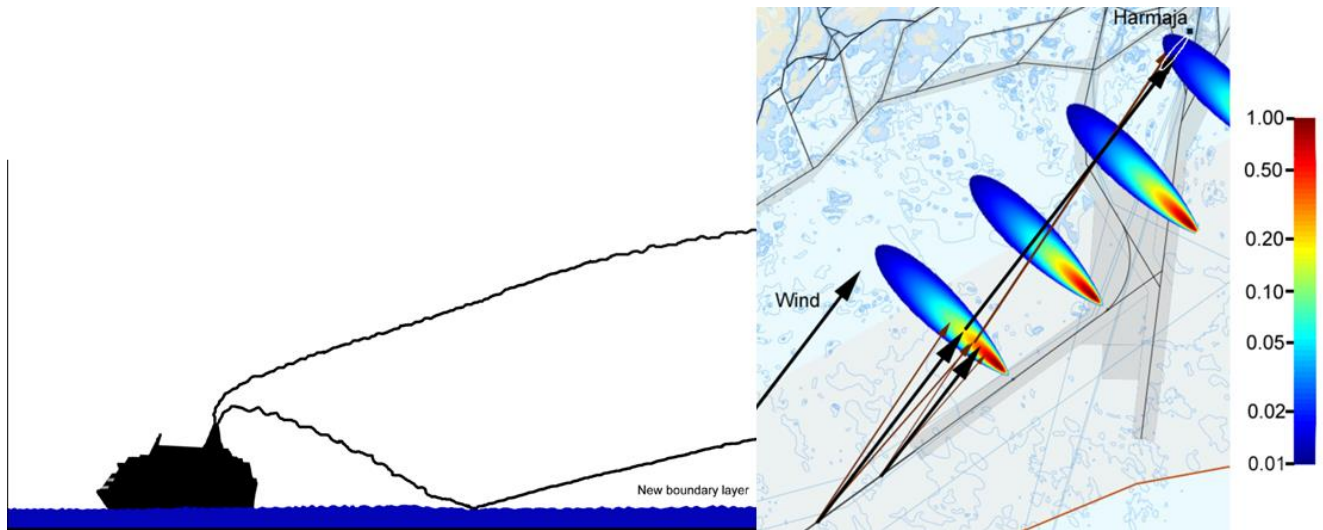
Figure 10. a) Schematic figure of the vertical profile of ship plume dispersion. If the stack height is around 55 m the plume touches the sea surface at around 450 m distance from the ship. b) The momentary plumes at 15, 23, 30 and 37 min after start (0 min) at the sea surface. Black arrows are the wind speed vectors (ws = 11 m s$^{-1}$), brown arrows show the dispersion of the plume and gray lines the ship routes to Helsinki, one passing Harmaja Island on its right side. Color on logarithmic scale (two decades, highest values dark red) refers to the pollutant
790 concentrations in the chimney. The footprint area, an ellipsoid in white color at Harmaja inside of which 80 % of flux is reached at the height of 10.7 m.

795
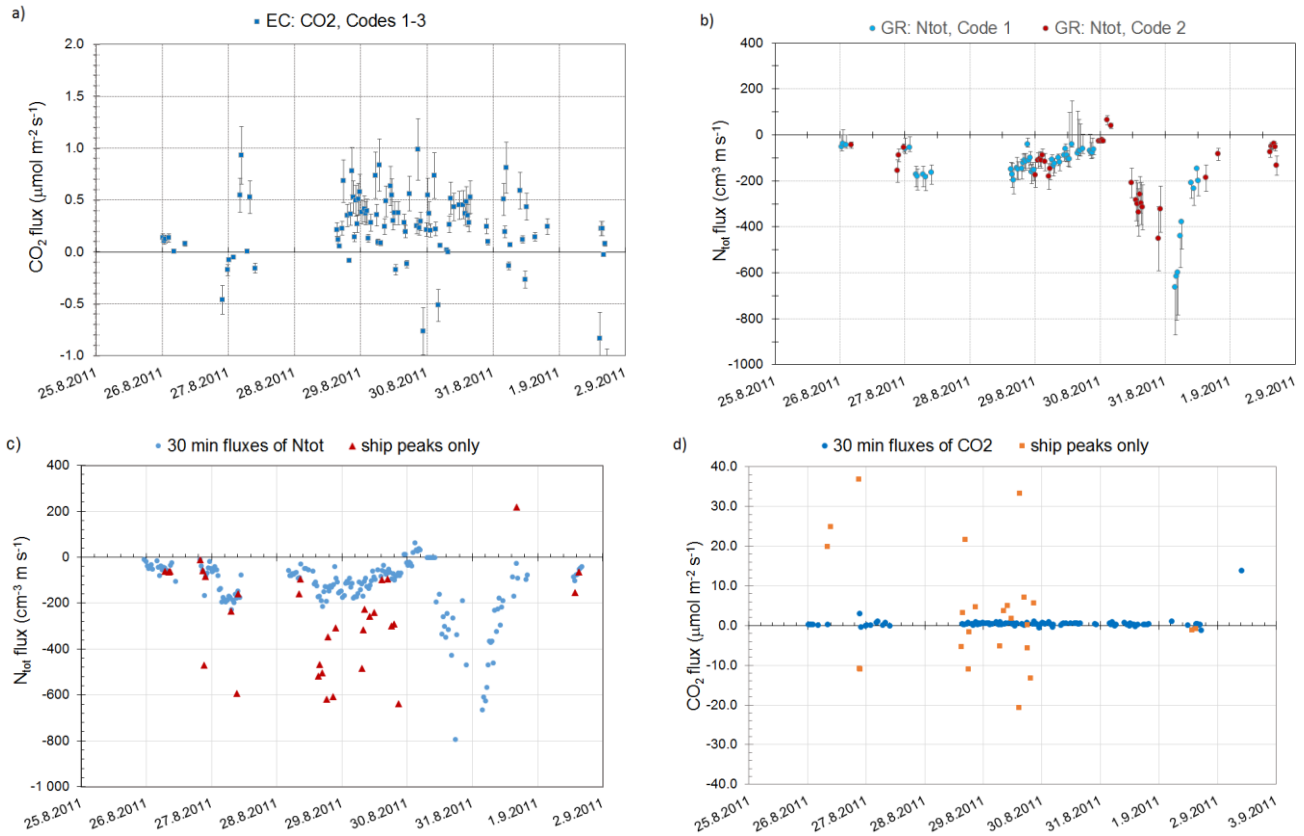
Figure 11. Time series of 30 min fluxes for $CO_2$ ($\mu$mol m$^{-2}$ s$^{-1}$) by the EC methods (a) in all wave conditions (codes 1 to 3), and $N_{tot}$ (cm$^{-3}$ m s$^{-1}$) by the GR method (b) with no swell (codes 1-2), along with the uncertainties. The data in (a) and (b) include only events in the wind sector between 150° and 270° and with the stationary criteria based on the momentum flux for Ntot and the $CO_2$ flux for CO2. c) Time

800   series of the 30 min fluxes of Ntot by the GR method in the wind direction of 150-270 °. Additionally, the fluxes of ship peaks are shown separately. d) The same as c) but for $CO_2$ fluxes.
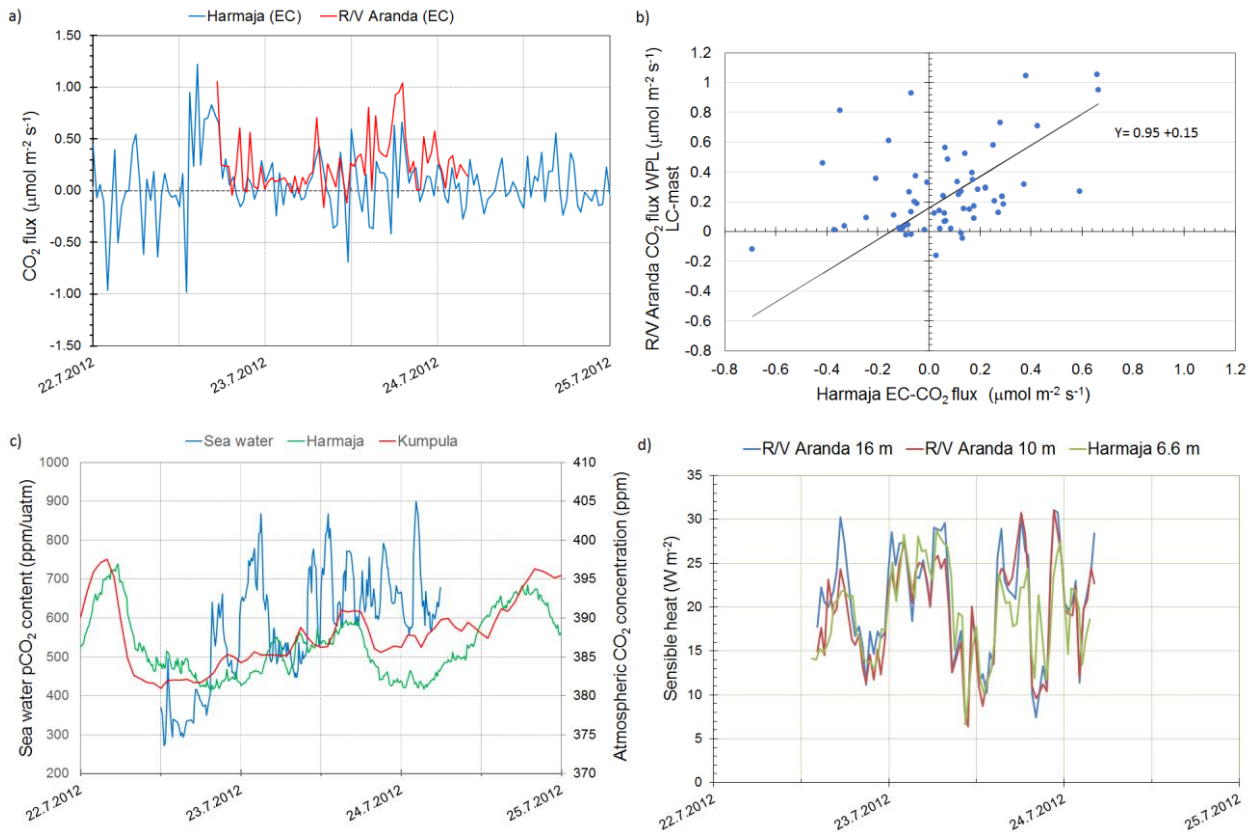
Figure 12. a) Time series of $CO_2$ fluxes by the EC methods in 2012 at Harmaja and at the R/V Aranda in the wind direction of 150-270°. b) Scatter plot of orthogonal regression analysis between EC-$CO_2$ flux measurements conducted at Harmaja and on R/V Aranda in 2012 Also presented if the ortogonal regression line. c) Partial pressure of $CO_2$ in the seawater from R/V Aranda, and $CO_2$ concentrations in the atmosphere at Harmaja and at the urban background monitoring station SMEAR III in Kumpula, Helsinki. d) Time series of sensible heat fluxes measured by the EC method at Aranda at 16 and 10 m altitudes and in Harmaja at 6.6 m altitude.
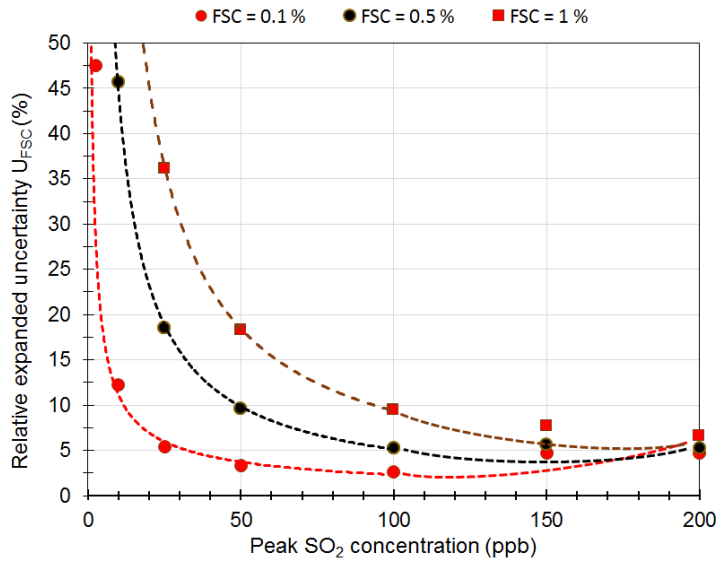
815    Figure 13. The expanded uncertainty of FSC, $U_{FSC}$ (%), as a function of $SO_2$ peak height concentration for three FSC limits: 0.1 % (red circle), 0.5 % (black circle) and 1 % (red square).
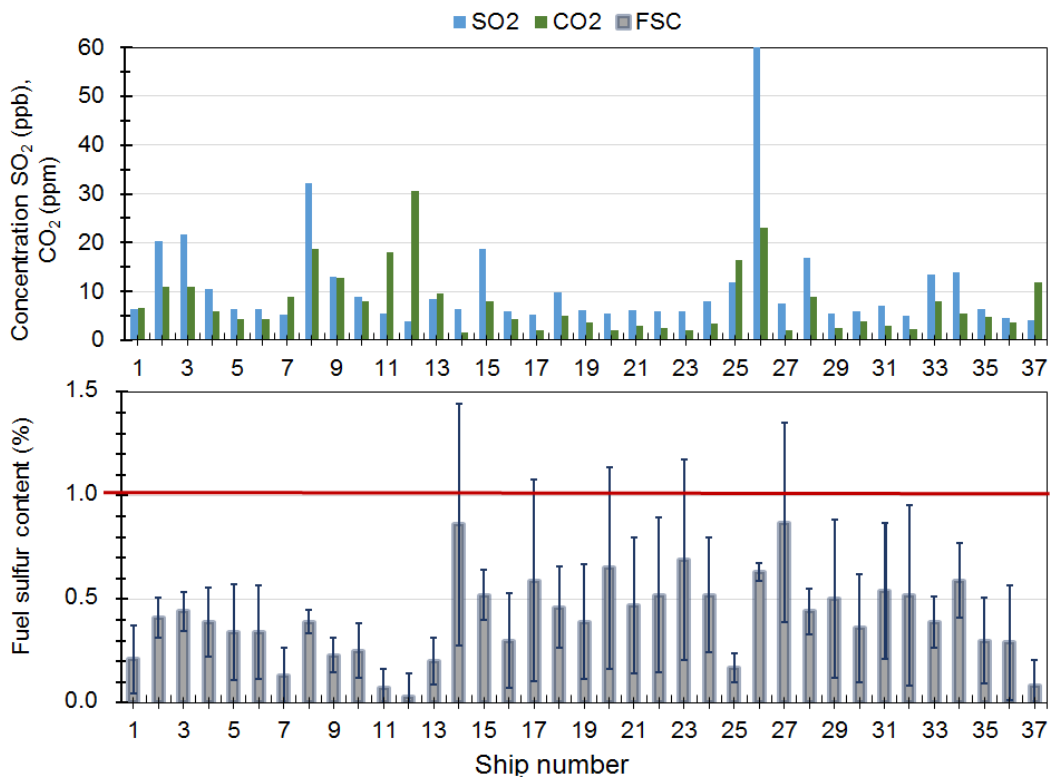
820     Figure 14. Peak height concentrations of $SO_2$ and $CO_2$ from a ship emission plume and calculated FSC with the expanded uncertainty $U_{FSC}$
during a short time period of the 2012 measurements. The red line represents the FSC = 1 % limit following the regulation (Directive
1999/32/EC). All the ships complied with the regulation.